

This is to certify that the

thesis entitled

AN EXPERIMENTAL DESIGN AND MODEL FOR THE
DISSOCIATION OF OXYGEN IN A MICROWAVE DISCHARGE

presented by

Jerome S. Wareck

has been accepted towards fulfillment
of the requirements for

M.S. degree in Chemical Engineering



Major professor

Date July 8, 1981



OVERDUE FINES:

25¢ per day per item

RETURNING LIBRARY MATERIALS:

Place in book return to remove
charge from circulation records

--	--

AN EXPERIMENTAL DESIGN AND MODEL
FOR THE DISSOCIATION OF OXYGEN IN A MICROWAVE DISCHARGE

by

Jerome S. Wareck

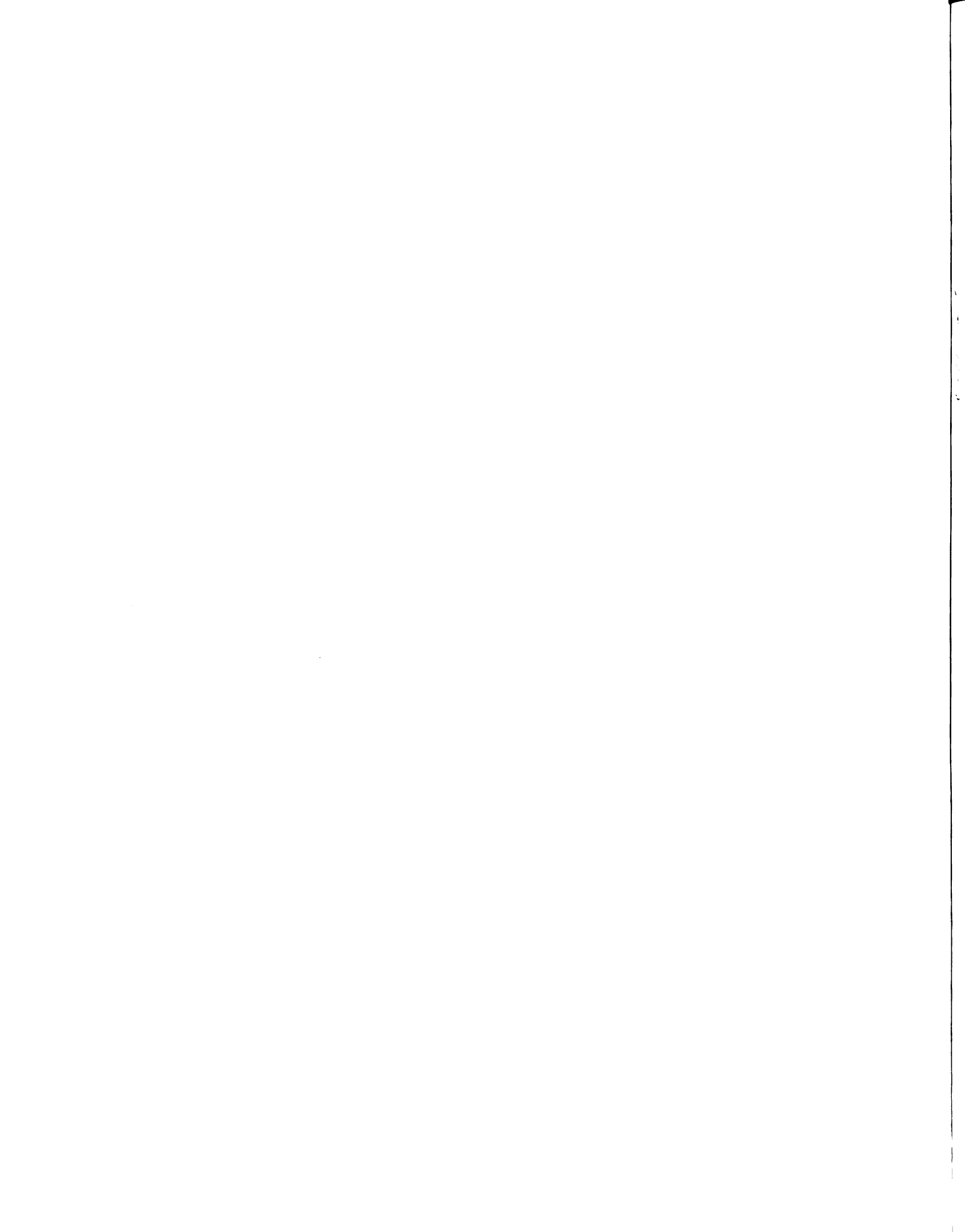
A THESIS

Submitted to
Michigan State University
in partial fulfillment of the requirements
for the degree of

MASTER OF SCIENCE

Department of Chemical Engineering

1981



ABSTRACT

An Experimental Design And Model
For the Dissociation of Oxygen in a Microwave Discharge

By

Jerome S. Wareck

6115671

A microwave plasma flow system for the generation and detection of atomic oxygen was developed. Preliminary experiments indicate high conversions of molecular oxygen to atomic oxygen are possible, with conversions of 9.3 and 4.0% for oxygen flow rates of 51.8 and 66.4 μ mole/sec, respectively, at a pressure of 3.4 torr. These conversions correspond to yields of 0.02478 and 0.01366 g mole/kw hr, respectively. Plug flow and CSTR models of the plasma were developed. Theoretical predictions of conversion and yield as a function of pressure, power, and flow rate were developed and compared to literature values. The results of the models agreed with the experimentally observed effects of flow rate and power density on conversion and yield, but predicted maxima in conversion and yield with increasing pressure at greater pressures than experimentally observed. This suggests that additional work is needed in determining how discharge parameters change with pressure and power density and that more detailed models be developed.

TO MY WIFE CHERYL, AND MY PARENTS SI AND JO WARECK

ACKNOWLEDGEMENTS

I would like to acknowledge the guidance of Dr. Martin C. Hawley, Dr. Jes Asmussen, Dr. Ronald Kerber, and the help of Reed W. Snellenberger in the design of the experimental program and Don Childs in the fabrication and construction of the system. I would also like to acknowledge the work of Mary Brake in the compilation of rate coefficient data and Pam Reynolds for her excellent work in preparing the manuscript.

TABLE OF CONTENTS

	<u>Page</u>
LIST OF TABLES	v
LIST OF FIGURES	vi
NOTATION	vii
INTRODUCTION	1
REVIEW OF PREVIOUS WORK	
Oxygen Atom Generation	3
Detection of Oxygen Atoms	8
Detection of O ₂ (¹ Δ _g)	11
DESCRIPTION OF EXPERIMENTAL PROGRAM	
Oxygen Flow System	13
NO ₂ Titration System	14
O ₂ (¹ Δ _g) Detection System	15
Plasma Cavity and Microwave System	16
Results and Discussion of Preliminary Experiments	17
THEORETICAL DISCUSSION AND MODELING	
Reactions of the Plasma	21
CSTR Model of the Plasma	23
Plug Flow Model of the Plasma	23
RESULTS AND DISCUSSION	
CSTR Model Results	25
Plug Flow Model Results	29
CONCLUSION	30
FUTURE WORK	32
REFERENCES	60
APPENDIX	
Fortran Listing of CSTR Model	65
Fortran Listing of Plug Flow Model	69

LIST OF TABLES

	<u>Page</u>
1. Summary of Oxygen Atom Generation Studies	33
2. Rate Coefficients for Neutral Collision Partners in O ₂ Dissociation	34
3. Surface Recombination Coefficient of Oxygen Atoms at 20°C	36
4. Summary of Preliminary Experiments	37

LIST OF FIGURES

	<u>Page</u>
1. Microwave Plasma Flow System	38
2. NO ₂ Titration Flow System	39
3. ¹ Δg (O ₂) Detection System	40
4. Conversion vs. Flowrate CSTR Model	41
5. Conversion vs. Flowrate CSTR Model	42
6. Yield vs. Flowrate CSTR Model	43
7. Yield vs. Flowrate CSTR Model	44
8. Conversion vs. Pressure CSTR Model	45
9. Conversion vs. Pressure CSTR Model	46
10. Yield vs. Pressure CSTR Model	47
11. Yield vs. Pressure CSTR Model	48
12. Effect of Pressure on CSTR Model Terms	49
13. Conversion vs. Power CSTR Model	50
14. Conversion vs. Power CSTR Model	51
15. Yield vs. Power CSTR Model	52
16. Yield vs. Power CSTR Model	53
17. Maximum Yield vs. Flowrate CSTR Model	54
18. Maximum Conversion vs. Power CSTR Model	55
19. Conversion vs. F/V Plug Flow Model	56
20. Conversion vs. F/V Plug Flow Model	57
21. Yield vs. F/V Plug Flow Model	58
22. Yield vs. F/V Plug Flow Model	59

NOTATION

D	diameter of discharge tube, cm
D_{O-O_2}	diffusivity of O in O ₂ , cm ² /sec
E	effective field strength, volts
F_O	flow rate of atomic oxygen, g mole/sec
$F_{O_2}^o$	flow rate of molecular oxygen to the plasma, g mole/sec
K_1	electron impact dissociation rate constant, cm ³ /sec
K_2	rate constant for reaction 2, cm ⁶ /sec
K_3	rate constant for reaction 3, cm ⁶ /sec
K_4	rate constant for reaction 4, cm ⁶ /sec
K_w	wall recombination rate constant, sec ⁻¹
m	mass of oxygen atom, g
m_e	mass of electron, g
N	total gas concentration, cm ⁻³
N_{av}	Avogadro's number, mole ⁻¹
n	atomic oxygen concentration, cm ⁻³
$\langle n_e \rangle$	volume average electron density, cm ⁻³
P	pressure, mmHg
\bar{P}	power density, watts/cm ³
R	gas constant
T	temperature, °K
T_e	electron temperature, °K
V_p	plasma volume, cm ³
V_r	random velocity from kinetic theory of gases, cm/sec
x	conversion
y	mole fraction of atomic oxygen
Y	yield of atomic oxygen, g mole/kw hr

GREEK LETTERS

γ	wall recombination coefficient for atomic oxygen on silica
ϵ	electron energy, ev.
κ	Boltzmann's constant, erg/ $^{\circ}$ K
Λ	diffusion length, cm
λ	wavelength, \AA
σ	total dissociation cross section, cm^2
τ	lifetime of excited species, sec.

INTRODUCTION

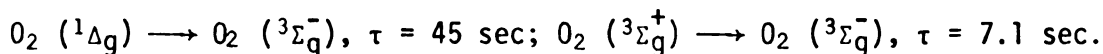
Several investigators have studied the dissociation of oxygen in a.c. discharges. Mearns and Morris¹, Brown³, and Williams and Mulcahy^{8,3} dissociated oxygen in microwave discharges; Bell and Kwong² and Battey⁴ dissociated oxygen in radiofrequency discharges. Their studies have shown the effect of pressure, power, flow rate, impurities, and coating of discharge and flow tubes, on the extent and efficiency of atomic oxygen production. In addition, Mearns and Morris¹, and Bell and Kwong² have developed models for the dissociation of oxygen which explain the experimentally observed effects of pressure, flow rate, and power on yield and conversion in terms of discharge parameters.

Currently there is interest in the possibility of using the energy evolved in the recombination of atomic species as a method of rocket propulsion. This interest has spawned a series of experiments designed to study the fundamental parameters in atom generation from molecules. Molecular gases such as oxygen and hydrogen will be dissociated in a microwave discharge and relations between discharge parameters and extent and efficiency of atom generation will be studied in detail and models will be developed. Inert gases will be studied in an effort to accurately determine electron density and temperature. The objective of this work was to design a flow system that yielded a high dissociation of oxygen and the means to detect oxygen atoms and an excited oxygen state, $O_2 (^1\Delta_g)$ that may be present in small amounts, in preparation for a detailed study of oxygen atom generation. This

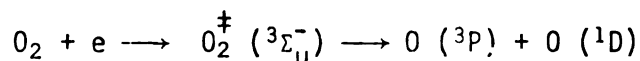
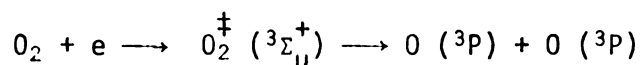
paper describes the experimental plasma system, experimental procedure, and preliminary results, as well as the difficulties encountered in the design. In addition, theoretical models of the oxygen plasma are presented and the effect of pressure, flow rate and power, on conversion and yield is discussed.

Table 1 summarizes the results of our studies of atomic oxygen generation listing specific experimental conditions and estimates of discharge parameters where possible. Also included is the flow rate of oxygen required to produce 1 lb of thrust for the conversion obtained in each case, and the scale factor for oxygen flow rate if the given conversion could be obtained with the flow rate required for 1 lb of thrust, under the given experimental conditions.

The ground state of the oxygen molecule is the ${}^3\Sigma_g^-$ state. The ${}^1\Delta_g$ state is 0.98 ev, and the ${}^1\Sigma_g^+$ 1.63 ev above the ground state. The lifetimes of the low lying excited state of oxygen are long:



Dissociation of molecular oxygen occurs by excitation to the ${}^3\Sigma_u^-$ or the ${}^3\Sigma_u^+$ states followed by dissociation to 3P or 1D states. The reactions are



The oxygen atom has three low lying states; the ground state is 3P , the 1D state is 1.967 ev and the 1S state is 4.188 ev above the ground state.

REVIEW OF PREVIOUS WORK

Oxygen Atom Generation

Mearns and Morris¹ have studied the dissociation of oxygen in a microwave discharge. Two cavities, coaxial and cylindrical, operating at 2450 MHz were employed. Discharges in silica tubes with 10 mm and 20 mm diameters were used. The effect of discharge residence time, pressure, power and discharge tube coatings were reported. Conversion increased with discharge residence time at constant pressure, and conversion decreased with increasing pressure at constant flow rate; conversions of 0-15% were reported for pressures of 2-5 torr. Oxygen atom yield decreased with increasing residence time at constant pressure, for powers of 208-218 W; yields ranged from 0.5 to 2.5 g atoms/kwhr. As pressure was increased at constant discharge residence time and absorbed power, the yield increased and conversion decreased (rapidly from 1 to 3 torr, less rapidly from 3 to 10 torr). Conversion increased linearly with absorbed power with moist oxygen having higher conversions than pure oxygen. Discharge tubes coated with orthophosphoric acid yielded higher conversions than non-coated tubes. Yield was constant as absorbed power increased. Conversion was higher for polytetrafluoroethylene-coated tubes than for non-coated tubes and conversion increased more rapidly with increasing power for coated tubes. A model was presented which expressed conversion in terms of discharge parameters.

Bell and Kwong² studied dissociation of oxygen in a radiofrequency discharge. A generator operating at 13.56 MHz, capable of delivering 150 watts, was connected to electrodes on flat ends of a Pyrex pillbox. Power varied from 0 to 140 watts, pressure from 2 to 4 torr and O₂ flow

rate from 2 to 10×10^{-4} moles/min. Conversions varied from 5 to 50%, yields from 0.05 to 0.20 g atoms/kwhr. In a stagnant discharge the atom concentration passed through a maximum at a fixed point in the reactor as pressure or power varied; the atom concentration was determined by the temperature differences between a catalytic (silver oxide) and a non-catalytic thermocouple. Conversion and yield (g atoms/kwhr) decreased with increasing pressure at constant power and flow rate (residence time increases with pressure). At fixed pressure and flow rate, dissociation increases for small increases in input power. The yield showed a maximum at 75 watts and decreased thereafter, this effect was more pronounced at lower pressures. Conversion decreased rapidly with increasing flow rate, again this effect being more pronounced at lower pressures where dissociation is highest. The yield was relatively insensitive to flow rate. It was observed that the gas temperature increased with power. The gas temperature increased with flow rate; this increase was attributed to a lower atom concentration which has a higher thermal conductivity than the molecule. A model was presented which included four homogeneous recombination reactions and wall recombination as well as estimates of electron density and average energy as a function of operating conditions. The model explains the observed effects of pressure, power and flow rate on conversion and yield.

Brown³ has investigated the effect of impurities on oxygen atom production in a microwave discharge. Power from a 2450 MHz source was varied from 4 to 85 watts, pressure from 0.52 to 1.2 torr and flow rate from 1.8×10^{-5} to 38×10^{-5} mole/sec. The effect of N_2 , H_2 , H_2O and O_2 on oxygen atom production was reported as a ratio of oxygen atoms produced/molecules of added gas. The oxygen atom concentration increased rapidly

as H

the

add

wit

pow

no

sup

si

st

in

w

t

o

n

f

f

e

as H₂O flow increased and leveled off when the flow of H₂O was 2% of the oxygen flow rate. A decrease in O₂ (¹Σ_g⁻) was observed as H₂O was added, due to increased dissociation. A slight decrease in O₂ (¹Δ_g) with increasing H₂O was also observed. For each flow rate there was a power range over which the atom concentration increased greatly with no further increase for high powers.

Batthey⁴ employed a radiofrequency generator operating at 13.56 MHz supplying up to 600 watts in a study of photoresist stripping from silicon wafers by an oxygen plasma. In an effort to determine the stripping rate as a function of pressure, power, and oxygen flow rate, information was obtained on how the atomic oxygen concentration changed with these parameters. He found that at constant pressure and power the flow of atomic oxygen increased linearly with the flow of molecular oxygen, i.e., no decrease in atomic oxygen concentration with decreasing residence time was observed. The atomic oxygen concentration was found to increase linearly with power and at pressures of 0.5 to 2.0 torr the first 50 watts were most effective in producing atomic oxygen. For an oxygen flow of 500 cc/min there was a maximum in atomic oxygen production around 0.5 torr for powers of 20, 100, and 200 watts, with the production decreasing with increasing pressure.

Bell⁵ has developed a general model for plasma reactions between two infinite parallel plate electrodes which includes continuity equations for charged and uncharged species and applied this model to an oxygen plasma. He included fifteen reactions including ionization, electron attachment, charge transfer, electron detachment, ion-ion recombination, dissociation, homogeneous and wall recombination. In this model, the species present are: electrons, atoms, positive ions,

and three negative ions (O^- , O_2^- , and O_3^-). It was assumed that the concentration of negative ions was controlled by homogeneous reactions, the loss of atomic oxygen was due to diffusion to the wall (modeled as a first order reaction) and that the electric field strength and electron density were uniform throughout the plasma. The model explained changes in species' concentration in terms of the rate constants and electron density. In a later paper Bell and Kwong⁶ modeled the data of Mearns and Morris¹ with a one dimensional plug flow model, neglecting axial and radial diffusion. Four homogeneous recombination reactions and wall recombination were included to account for the loss of atomic oxygen. In modeling the coaxial cavity (discharge volume 2-3 cc) the theory was 20 to 30% lower than the data but followed the trends for variation of conversion and yield with pressure. At 1 torr the model followed the trend of increased conversion with increasing power, but at 4 torr the theory predicted a more rapid rise in conversion with power than the data exhibited. They incorporated a linear temperature rise for the gas and the wall into the model to account for this, which caused the rate of dissociation to decrease and the rate of recombination to increase. In modeling the cylindrical cavity (discharge volume 70 cc) the theory predicted a more rapid decrease in conversion and yield with increasing flow rate than the data exhibited. This was explained by an overestimation of dissociation at low pressures which is supported by the fact that the slopes of conversion and yield vs. flow rate for the theory and data were more consistent at higher pressures. Finally, the model had near perfect agreement with the data in variation of conversion and yield with power for the cylindrical cavity.

Kaufman⁷ reviewed the basic physical processes that occur in d.c. and a.c. glow discharges and applied these concepts to H₂, N₂, O₂ dissociation, ionization, and recombination.

Hake and Phelps⁸ calculated momentum-transfer and inelastic cross sections for electrons in O₂, CO, and CO₂ from measured values of the electron drift velocity, characteristic energy, attachment coefficient, and ionization coefficient.

Extensive investigations have been made of kinetic mechanisms of homogeneous reactions of oxygen gas mixtures with both simple and complex molecules. A summary of rate coefficients for the neutral species reactions of oxygen gas mixtures is given in Table 2. All rate constants are evaluated at 300°K unless noted otherwise and have units cm³/molecule-sec or cm⁶/molecule²-sec. Schofield⁶⁴ has reviewed the rate constants through mid-1972 for various gas phase reactions and evaluated their accuracy. Elias and Schiff⁶⁵ determined absolute rate constants for oxygen atom reactions with ethylene and butane. Westenberg and De Haas⁵² studied the kinetics of atomic oxygen reactions with hydrogen, methane, and ethane. Bonanno, Kim, Lee, and Timmons⁶⁶ determined the rate constant for the reaction of atomic oxygen with benzene. Herron and Penzhorn⁶⁷ investigated the reactions of atomic oxygen with ethylene and formaldehyde. Herron and Huie^{68,69} determined rate constants for reactions of atomic oxygen with C₁ to C₅ alkanes.

A survey has been made of kinetic mechanisms for the charged particle species in an oxygen discharge. A listing of these mechanisms and their associated rates is given in Table 3. This segment of mechanism survey is not complete. Further work is required to completely evaluate the status of this data.

Greaves and Linnett^{76,77,78} studied the recombination of oxygen atoms on metal, non-metal, oxide, halide surfaces and on silica surfaces from 20° to 600°C. Linnett and Marsden^{79,80} reported recombination coefficients for oxygen atoms on Pyrex, salt, and oxide surfaces over a temperature range of 20° to 400°C. Kaufman⁸¹ has reviewed surface recombination coefficients of oxygen atoms on various materials. A compilation of the surface recombination coefficients for oxygen atoms is given in Table 4.

The generation of oxygen atoms for use in reactions requires minimization of atom wall recombinations before atoms reach the reaction zone. This requirement has motivated the study of wall coatings that reduce wall recombination. Williams and Mulcahy⁸³ investigated the effect of various coatings on recombination of oxygen atoms on glass. They studied the effects of Teflon, a silicone resin, Dri-film (dichlorodimethylsilane and methyltrichlorosilane), orthophosphoric acid, sulfuric acid, boric oxide, and polymethylmethacrylate. In the experiment oxygen passed through two parallel tubes, one a control tube coated with Teflon. Oxygen atoms were generated by a microwave discharge and then entered the two parallel tubes. Nitrogen present in the oxygen provided an air-afterglow, the intensity of which was monitored at three to five points along the flow tube. Sulphuric acid was the only material found to have a lower recombination coefficient than acid-washed glass. Dri-film and orthophosphoric acid had essentially the same recombination coefficient as acid-washed glass.

Detection of Oxygen Atoms

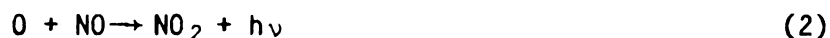
Kaufman⁸¹ has reviewed four methods for the measurement of oxygen atom concentration, evaluating the advantages and disadvantages of each.

One method is the use of catalytic probes. A thermocouple or wire is coated with silver (which has a very large recombination coefficient for oxygen atoms) and placed in the gas stream. Atoms recombining on the probe heat it; in the case of thermocouples, the e.m.f. readings are proportional to the atom concentration; in the case of a coated wire, the difference in electrical power to produce the same wire temperature in the presence and absence of oxygen atoms is measured and flow of atomic species is proportional to the difference in current squared.

Another method is the use of Wrede-Harteck Gauges. The pressure difference between the discharge gas and a small chamber coated with a catalytic material is measured. Both atoms and molecules enter the chamber; the atoms recombine and only molecules exit. The pressure difference is proportional to the fraction of atoms present.

A third method is electron spin resonance. Westenberg and De Hass⁵² reviewed the general theory relating intensities of ESR absorption to concentrations and then applied the theory to the determination of oxygen, nitrogen, and hydrogen atom concentrations.

The fourth method reviewed by Kaufman^{81,84} is nitrogen dioxide titration and air afterglow. These methods depend on the two reactions



and on the fact reaction 1 is much faster than reaction 2 ($K_1 = 3 \times 10^{-12}$ and $K_2 = 1 \times 10^{-17} \text{ cm}^3/\text{molecule-sec.}$). In the air afterglow method a little NO is added to a stream containing oxygen atoms. A green glow is produced the intensity of which is proportional to the oxygen atom concentration. The decrease in intensity of the glow along a flow tube is equal to the decay of oxygen atoms.

In NO_2 titration, NO_2 is added downstream of the discharge and a bright green glow is produced. As the flow rate of NO_2 is increased the intensity of the glow increases to a maximum, when the NO_2 flow rate is one-half the oxygen atom flow rate. As the NO_2 flow rate is further increased the intensity of the glow decreases, as more and more oxygen atoms are removed by reaction 1. At the endpoint of the titration, all oxygen atoms are removed by reaction 1 and the glow is extinguished. Mearns and Morris⁸⁵ point out that at pressures greater than about 2 torr the sharpness of the endpoint decreases rapidly with increasing pressure due to reaction 3



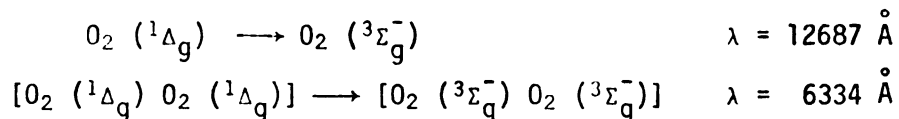
which, followed by reaction 1, produces a gradient in the afterglow intensity. Mearns and Morris⁸⁵ give suggestions for the use of NO_2 titration up to 10 torr.

Once the endpoint is reached, the NO_2 flow rate must be found. Kaufman⁸¹ suggests measuring the pressure drop of the NO_2 - N_2O_4 equilibrium mixture at low pressures (20 to 50 torr) in a known volume. Another method is to measure the weight loss of NO_2 generated from liquid N_2O_4 in an ice bath. Westenberg and De Haas⁵² calculated the NO_2 flow rate by timing a measured pressure rise in a known volume.

At 70°F and 1 atm the equilibrium between N_2O_4 and NO_2 is such that the vapor is about 29% NO_2 and 71% N_2O_4 . At 0.5 atm and 70°F the composition is about 38% NO_2 and 62% N_2O_4 . At low pressures (less than 10 torr) greater than 90% of the vapor is NO_2 . Therefore, under certain conditions, corrections for the NO_2 - N_2O_4 equilibrium might be necessary. The papers of Verhoek and Daniels⁸⁶, Steese and Whittaker⁸⁷, Seshadri, Fiswanath, and Kuloor⁸⁸, and Giaque and Kemp⁸⁹ provide useful thermodynamic properties of the NO_2 - N_2O_4 equilibrium.

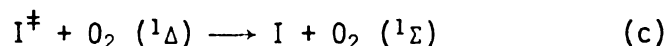
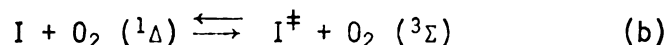
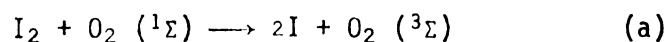
Detection of O_2 ($^1\Delta_g$)

Two methods of determining the concentration of O_2 ($^1\Delta_g$) are described here. The first method directly monitors the intensities of transitions from single and double molecule states to the ground state:



An infrared detector is fitted with filters to isolate the spectral regions of concern. The intensity measured can be related to absolute or relative O_2 ($^1\Delta_g$) concentrations.

The second method involves electronic energy transfer between O_2 ($^1\Delta_g$) and dissociated iodine, with subsequent fluorescence of the excited iodine to the ground state; Arnold, Finlayson, and Ogryzlo⁹⁰, reported a bright yellow-green glow, visible even in room light, when iodine vapors were introduced into a discharged oxygen stream. Derwent and Thrush^{91,92} studied the kinetic behavior, vibrational distribution, absolute intensity, and lifetime of the excited iodine and its emission. They determined that the chemiluminescence arises from the following reactions:



Small amounts of added iodine (<0.01%) are almost completely dissociated and any I_2 formed by heterogeneous recombination of the iodine atoms is again dissociated by O_2 ($^1\Sigma$). The result is a constant concentration of iodine atoms downstream from the injection point. Derwent and Thrush⁹¹ found that the intensity of the chemiluminescence arising from reaction (d) showed a maximum around 5800 Å and was proportional to the total iodine concentration and to the concentration of O_2 ($^1\Delta_g$). By measuring the intensity of the glow, absolute or relative O_2 ($^1\Delta_g$) concentrations can be determined. Wayne⁹³ has reviewed other methods of singlet oxygen detection.

DESCRIPTION OF EXPERIMENTAL PROGRAM

Oxygen Flow System

The microwave plasma flow system is shown in Figure 1. The discharge occurred in a quartz tube of 8 mm ID. An 18 mm ID tube was available as well as two tubes arranged for annular flow. The annular flow tubes were arranged with a 30 mm OD tube fused at both ends through the wall of a 37 mm ID tube and a 20 mm tube fused at both ends through the wall of a 28 mm ID tube. Provisions were made to introduce a cooling air jet through this inner tube to keep wall temperature low and thus keep wall recombinations low. At high flow rates the plasma is seen to move toward the walls of the tube which means that a large fraction of the gas passes through the plasma zone without being excited. It is believed that by confining the plasma to an annular region this bypassing may be eliminated and conversion increased.

All tubes were fitted with a ground quartz joint to connect with the vacuum system downstream of the discharge. Prior to use all tubes were placed in a dilute hydrogen fluoride bath for several minutes and then rinsed with distilled water. The ends of unused tubes were sealed with Parafilm to keep contaminants out.

Two purities of oxygen were available: 95% O₂, 5% CO₂, and 99.995% O₂. For these preliminary experiments the less pure oxygen was used. The oxygen was passed through calibrated Matheson rotameters (types 601 and 602) to a needle valve that controlled the feed rate. In the calibration of the rotameters, the oxygen regulator was set at 20 psig and delivered to the rotameters at this pressure. A needle valve directly

downstream of the rotameter throttled this pressure to 1300 torr as measured by a Heise gauge.

The rotameters were calibrated by bubbling the gas into an inverted graduate cylinder filled with water. Recordings of volume of water displaced versus time were taken for several rotameter settings. An average of three or four such measurements were made for each setting. With the two rotameters oxygen flow rates of 4 to 800 $\mu\text{moles/sec}$ were possible.

The known flow rate of oxygen was then passed through the microwave cavity. Pressure readings were taken upstream and downstream of the discharge. The cavity was tuned by varying the length until maximum incident power and minimum reflected power was obtained.

After the discharge region the gas entered 2 inch ID Pyrex pipe which comprised the remainder of the vacuum system. The discharge gas was titrated with NO_2 at three points downstream at distances of 13 cm, 31 cm, and 83 cm from the discharge exit. The injectors were constructed of Pyrex with pepperpot type holes pointed downstream and connected to the vacuum system by means of ground glass joints, these being non-metal to prevent microwave leakage into the laboratory and atom recombination. The discharge pressure could be adjusted by a valve downstream of the cavity, keeping flow rate constant.

NO_2 Titration System

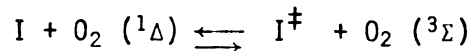
The NO_2 titration system is shown in Figure 2. A cylinder of liquid $\text{N}_2\text{O}_4\text{-NO}_2$ was connected to a small stainless steel reservoir that acted as a capacitor, keeping liquid out of the system. The effluent gas from the reservoir was connected to a needle valve upstream of the flow control needle valve to limit the backpressure to a Matheson type 610 rotameter. NO_2 backpressure to the flow control needle valve was

measured downstream of the rotameter and upstream of the flow control valve. Downstream of the flow control valve was a three-way directional valve that could direct NO_2 to the system for titration or to a reservoir of known volume for calibration.

The NO_2 backpressure was monitored to assure that a constant flow rate had been obtained. The NO_2 stream was then directed to a known volume and the pressure rise timed. The pressure was measured by a Penwalt Wallace Tiernan gauge with gradation every 0.2 torr. A minimum of eight increments or two or three minutes was allowed for each calibration. The pressure in the known volume was kept below 10 torr while the backpressure to the flow control valve was typically 200 torr, assuring choke flow into the volume. The pressure-time points could then be least-squares fit to a straight line and dP/dt determined from the slope. The flow rate of NO_2 is then given by $m=V/RT(dP/dt)$. Correlation coefficients for these lines were typically 0.999 or better indicating that the flow was indeed choked. After the plasma had been operating for a few minutes and reached a steady power level, NO_2 titrations were performed. NO_2 was introduced into the appropriate injector and adjusted until the glow was extinguished. An average of three titrations determined the oxygen atom flow rate, allowing a few minutes between titrations for any residual NO_2 to be drawn off. A photomultiplier tube was available for determining the endpoints at higher pressures where the endpoint is less sharp.

$\text{O}_2(1\Delta_g)$ Detection System

The $\text{O}_2(1\Delta_g)$ detection system is shown in Figure 3. The system utilizes the near resonant gas kinetic transfer of energy between molecular oxygen and atomic oxygen by the process:



Since the process is very rapid and nearly resonant, the final I^\ddagger population may be directly related to the $O_2 (^1\Delta_g)$ population. To perform this measurement twenty four inches of 2 inch ID Pyrex pipe was partially filled with iodine crystals. A helium tank was connected to this pipe so that iodine molecules could be introduced into the system in a helium stream. The backpressure of the helium-iodine stream was measured by a Hg manometer upstream of the flow control valve. Prior to detection the iodine crystals were heated to approximately 60°C to increase the vapor pressure and thus allowing more iodine to be introduced. Since $O_2 (^1\Delta_g)$ has a long life time (45 sec.), the iodine was introduced into the injector farthest from the cavity to avoid contamination of the system where NO_2 titrations were performed. The intensity of the glow is directly proportional to the $O_2 (^1\Delta_g)$ concentration.

Plasma Cavity and Microwave System

The quartz discharge tube is situated along the axis of the cylindrical microwave cavity. The cavity has an ID of 20.3 cm and can be adjusted to a maximum length of 34 cm. Externally soldered tubing coils allow the cavity to be water cooled. The quartz tube is cooled by an air jet directed into the cavity. A screened viewing port is situated in the wall of the cavity allowing observation of the plasma.

The cavity can be operated in a number of different modes depending on the type of probe used, the distance the probe is inserted into the cavity, and the cavity length. A probe coupling is used to excite the TE^*_{112} or TE_{011} modes and a loop coupling is used to excite the TM_{011} mode. Adjusting the cavity length allows maximum power to be absorbed

by the plasma, the optimum length being determined by the cavity mode and the plasma pressure. In these experiments the TE 011 mode was used with a cavity length of 9.5 cm.

The microwave source is a fixed frequency, 2.45 GHz magnetron oscillator capable of delivering 1400 watts. The power is incident on a power divider allowing a continuously varied power from near zero to full magnetron output. The power from the divider passes through a circulator, through incident and reflected directional couplers, and is directed into the plasma cavity by means of the probe or loop couplings mentioned earlier. The power reflected from the cavity passes through the circulator and is absorbed by a dummy load attached to a third port on the circulator. This prevents the magnetron from being exposed to large amounts of reflected power that can be present while tuning the cavity. The power absorbed by the plasma was assumed to be the difference between the incident and reflected power as measured through the directional couplers. Wall losses are assumed to be negligible, which may not actually be the case, however, The microwave system has been described in detail in earlier papers^{94,95}.

Results and Discussion of Preliminary Experiments

Many designs of the experimental setup were investigated in pursuit of a system that yielded detectable conversions of atomic oxygen. Each design and the problems encountered with each variation are described below.

The first design of the quartz plasma tube had aluminum flanges on either end of the tube sealed to the vacuum system by means of O-rings. The injectors for NO₂ titration, were coarse glass spargers connected to the vacuum system by means of ground glass joints. The plasma tube was

U

a 28 mm ID quartz tube. Table 5, design a, lists results of these experiments. It can be seen from this table that conversions were extremely low, all less than 0.5%. Since a large diameter tube and relatively high flow rates were being used, it was suspected that the low conversions were due to significant bypassing. A window was installed on the upstream end of the discharge tube so that the plasma could be viewed by looking up the axis of the tube. It was observed that the plasma was confined to a small annular region near the tube wall, indicating substantial bypassing, even at relatively low flow rates (70-100 μ mole/sec). An 18 mm ID quartz tube was installed and greatly expanded the flow range before bypassing was observed. The results, however, were only slightly better than with the 28 mm ID tube with conversions still less than 1%.

During the course of these experiments it was observed that the aluminum connection downstream of the discharge became quite warm, indicating that excessive wall recombinations were occurring on the aluminum. Greaves and Linnett⁷⁷ report a recombination coefficient of oxygen atoms on aluminum an order of magnitude larger than that on silica. A method was sought for resolving this problem. Two solutions became apparent: coating the aluminum or removing it entirely and replacing it with glass. Williams and Mulcahy⁸³ reported coating glass with Dri-film, a mixture of dichlorodimethylsilane and methyltrichlorosilane in a solvent, now produced by Silar Laboratories. Upon exposure to moist air, the solvent and the silanes evaporate, the chlorine groups on the silanes are hydrolyzed forming HCl, and a silane polymer is formed on the surface. This material was applied to the aluminum and was found to oxidize the surface and to weakly adhere.

Experiments were performed with the silane-coated flanges and conversions in the range of 0.75 to 1.50% were obtained for oxygen flow rates in the range of 30 to 350 $\mu\text{mole/sec}$. The silane polymer was then applied to the aluminum surface while the pieces were connected since some of the polymer might have been removed during construction of the system. The results of experiments subsequent to this showed conversions of 1.5 to 3.0% for the same flow rate range.

The aluminum was still observed to warm during experiments, indicating wall recombinations were occurring; however, the Dri-film did improve conversion. The aluminum connection was then replaced with ground quartz connections thereby removing all recombinations due to the aluminum, and at the same time an 0.8 mm ID tube was installed which would increase the power density and allow a high oxygen flow rate before bypassing. Results of these experiments are shown in Table 5, design b. The conversions were still excessively low when compared to literature values.

The injectors used thus far were coarse glass spargers which injected NO_2 both upstream and downstream. By injecting NO_2 upstream an unknown number of oxygen atoms were removed before reaching the titration point as evidenced by the presence of a glow upstream for a large distance. New injectors were designed and installed which were shaped with a bulb on the end with pepperpot type holes on one side of the bulb. Results of experiments with these injectors were slightly better than those with sparger injectors, with conversions of 2-3% for the same flow rate range. The NO_2 glow was still seen to extend slightly upstream at end point meaning either a diffusion or pressure drop problem was being encountered. Lowering the backpressure of the NO_2 , thereby injecting

NO₂ at a lower pressure was ineffective. The NO₂ was being injected into a 2 inch ID Pyrex pipe downstream of the discharge. The discharge was occurring in a 0.8 mm tube meaning that at a fixed oxygen flow rate the pressure in the cavity was higher than that in the 2 inch ID pipe downstream. By reducing the diameter of this section of pipe to 1 inch ID less pressure drop would occur from discharge tube to flow tube.

Prior to installation of the one inch downstream pipe, experiments were conducted with injectors pointed upstream, towards the discharge. The endpoints were very sharp with no glow at all present at the endpoint. Conversions were 3.8% and 2.8% for oxygen flow rates of 32.5 and 283.6 μ moles/sec, respectively.

Experiments conducted with the coated one inch diameter downstream pipe, injectors pointed downstream yielded conversions of 4.0% and 9.3% for oxygen flow rates of 66.4 and 51.8 μ mole/sec respectively, which are in the range of conversions obtained by other investigators at this pressure (3.4 torr). By lowering the pressure delivered to the rotameters (which was at 20 psig for these experiments) lower discharge pressure will be possible, which should increase conversion according to other investigators^{1,2,5,6}.

Early experiments in O₂ (¹ Δ_g) detection also encountered problems. When iodine molecules are added to a gas containing O₂ (¹ Δ_g) there is an energy transfer from the excited oxygen to the iodine which then fluoresces in the visible range. The intensity of the glow can be measured by a photomultiplier tube and relative concentrations of O₂ (¹ Δ_g) can be determined from one set of experimental conditions to another. No quantitative results of O₂ (¹ Δ_g) yield have been made at this time.

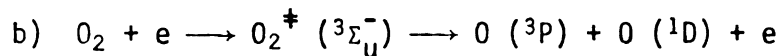
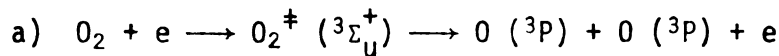
U

THEORETICAL DISCUSSION AND MODELING

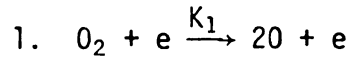
Reactions of the Oxygen Plasma

The plasma zone can be modeled either as backmix or plug flow reactor depending on the magnitude of the Peclet number, $K_1 \langle n_e \rangle D_{O-O_2} / V_r^2$, which is a measure of the axial dispersion in a flow reactor. For $Pe \ll 1$, axial dispersion is an important transport mechanism and the resulting internal mixing is best described by a backmix reactor model. Both models are developed on the following pages.

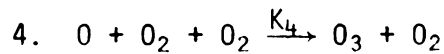
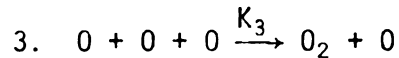
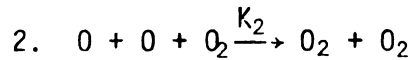
Molecular oxygen is dissociated after excitation by collision with high energy electrons:



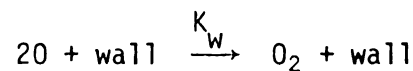
where ${}^3\Sigma_u$ states are excited states. In the model developed these two paths are combined into one:



There are three major homogeneous recombination reactions that result in loss of atomic oxygen.



Finally, atomic oxygen can be lost by heterogeneous wall recombination:



Bell^{2,6} has calculated the rate constant for electron impact dissociation of molecular oxygen. The rate constant can be determined from the expression:

$$K_1 = \sqrt{\frac{8}{\pi m_e}} (\kappa T_e)^{-3/2} \int_0^{\infty} \epsilon \sigma(\epsilon) \exp(-\epsilon/\kappa T_e) d\epsilon$$

where m_e is the mass of an electron, T_e is the electron temperature, ϵ is the electron energy, and σ is the total dissociation cross section. This equation assumes that the electron energies follow a Maxwell-Boltzmann distribution. Bell^{2,6} has prepared plots of K_1 vs. E/P , where E/P is the ratio of effective field strength to gas pressure, since the average electron energy can be related to E/P . Bell^{2,6} also has provided plots of E/P and $\langle n_e \rangle / \bar{P}\Lambda$ vs. $\bar{P}\Lambda$, for oxygen at 25°C where $\langle n_e \rangle$ is the volume average electron density, \bar{P} is the power density, and Λ is the diffusion length, $\Lambda = R/2.405$ (the radius divided by the first zero of the zero order Bessel function) for cylindrical flow. Bell's development shows that E/P and $\langle n_e \rangle / \bar{P}\Lambda$ are functions only of $\bar{P}\Lambda$.

Rate constants for the homogeneous recombination reactions are taken from Table 1. The wall recombination rate constant can be calculated from:

$$K_w = \frac{V_r \gamma}{2D}$$

where γ is the wall recombination coefficient, D the diameter of the flow tube, and V_r is the random velocity from kinetic theory of gases.

$$V_r = \left(\frac{8\kappa T}{\pi m} \right)^{1/2}$$

where κ is Boltzmann's constant, T is the gas temperature and m is the mass of the particle. The recombination coefficient, γ was taken to be 1.6×10^{-4} as determined by Greaves and Linnett⁷⁸.

CSTR Model of the Plasma

The material balance on atomic oxygen in the steady-state backmix reactor model yields:

$$-F_o N_{av} + r_o V_P = 0 \quad (5)$$

$$\text{where } r_o = 2K_1 \langle n_e \rangle [O_2] - 2K_2 [O]^2 [O_2] - 2K_3 [O]^3 - K_4 [O][O_2]^2 - 2K_w [O] \quad (6)$$

Defining a conversion $X = 0.5 F_o / F_{o_2}^o$ allows rewriting (5)

$$\begin{aligned} -2F_{o_2}^o N_{av} X + \left[2K_1 \langle n_e \rangle N \frac{(1-X)}{(1+X)} - 2K_2 N^3 \left(\frac{2X}{1+X} \right)^2 \left(\frac{1-X}{1+X} \right) - 2K_3 N^3 \left(\frac{2X}{1+X} \right)^3 \right. \\ \left. - K_4 N^3 \left(\frac{2X}{1+X} \right) \left(\frac{1-X}{1+X} \right)^2 - 2K_w N \left(\frac{2X}{1+X} \right) \right] V_P = 0 \end{aligned}$$

This equation can now be solved by a numerical technique to determine conversion as a function of flow rate, pressure, and power density. The yield can be calculated from

$$Y = 7.2 \times 10^6 F_{o_2}^o X / \text{Power gmole/kwhr}$$

Plug Flow Model of the Plasma

The material balance for the plug flow reactor model yields:

$$N_{av} \frac{dF_o}{dV} = r_o \quad (7)$$

where r_o is given by equation (6).

Equation (6) can be written as

$$r_o = 2K_1 \langle n_e \rangle [N-n_o] - 2K_2 n_o^2 [N-n_o] - 2K_3 n_o^3 - K_4 n_o [N-n_o]^2 - 2K_w n_o$$

Defining a conversion $X = 0.5 F_o / F_{o_2}^o = n_o / (2N - n_o)$ and a mole fraction

$$y = n_o / N = 2X / (1+X)$$

$$\begin{aligned} \frac{4F_{o_2}^o N_{av}}{N(2-y)^2} \frac{dy}{dV} = 2K_1 \langle n_e \rangle (1-y) - 2K_w y - 2K_2 N^2 y^2 (1-y) - 2K_3 N^2 y^3 \\ - K_4 N^2 y (1-y)^2 \end{aligned} \quad (8)$$

U

Equation 8 can now be numerically integrated to determine mole fraction, and, therefore, conversion as a function of flow rate, volume, pressure, and power density. In this study, the power density, flow rate, and conversion were specified and the plasma volume required to achieve this conversion was calculated. The conversion and yield are then presented vs F/V_p .

RESULTS AND DISCUSSION

CSTR Model Results

The effect of flow rate on conversion for pressures of 0.33 and 0.67, torr, respectively, at four power densities is shown in Figures 4 and 5. It can be seen that conversion decreases with increasing flow rate. Increasing the flow rate decreases the residence time in the plasma as seen by

$$t = PV_p / [RT (F_{O_2}^\circ - 0.5 F_o)] = PV_p / [RTF_{O_2}^\circ (1-x)]$$

If Equation (5) is written in terms of conversion and solved for $F_{O_2}^\circ$ and the conversion is allowed to increase, $F_{O_2}^\circ$ must decrease. Therefore for increasing $F_{O_2}^\circ$, conversion must decrease for the equality to hold. This effect has been observed in the literature^{1,2,5,6}. As the power density increases the rate of conversion increases at a higher flow rate. Increasing power density increases the electron density and more molecules are dissociated at a given flow rate. As the flow rate becomes small, the slopes of the curves approach infinity since the generation mechanism becomes much larger than the loss mechanisms. The linear portion of the plots extends over a greater flow rate range as pressure increases because the loss mechanisms increase with pressure at a higher rate than the generation mechanism, meaning that generation and losses are balanced over a larger flow rate range at higher pressures.

Figures 6 and 7 show the effect of flow rate on yield (expressed as gmole/kwhr) for pressures of 0.33 and 0.67 torr, respectively, at four power densities. Initially, the yield increases rapidly with flow rate and approaches a maximum value at high flow rates. At low flow rates conversion is high but fewer oxygen atoms are formed per kilowatt hour.

As the flow rate increases more oxygen atoms are formed, thereby increasing the yield. At high flow rates the yield approaches a maximum since the rate of oxygen atom production becomes nearly constant as can be seen by Figures 4 and 5. Mearns and Morris¹ report a linear increase in yield as flow rate increases for pressures of 2-5 torr while Bell and Kwong² report yield to be insensitive to flow rate for pressures of 2-3 torr. The yield increases as power density decreases since the rate of oxygen atom production increases more slowly than does the power input. Comparing Figures 6 and 7 shows that the yield increases more rapidly with flow rate as pressure decreases for very low flow rates but approach lower asymptotic values as flow rate increases. This is due to a decrease in conversion as pressure decreases in this pressure range.

Figures 8 and 9 show the effect of pressure on conversion at oxygen flow rates of 100 and 200 $\mu\text{mole/sec}$, respectively, at three power densities. At both flow rates the conversion reaches a maximum and then decreases with increasing pressure. As pressure increases E/P and $\langle n_e \rangle$ decrease and, moreover, the rate constant for the electron impact dissociation of oxygen, K_1 , decreases. Examining the material balance on atomic oxygen (Equation 5) one would expect conversion to decrease with increasing pressure since the homogeneous reaction terms in the rate equation increase with pressure to the third power and the product $K_1 \langle n_e \rangle$ decreases with increasing pressure. Figure 12 is a plot of the magnitude of the terms in the rate equation as a function of pressure for the conditions of curve 1 in Figure 6. This plot shows that the electron impact dissociation term increases slowly with pressure. An examination of the terms shows that the product $K_1 \langle n_e \rangle$ decreases more slowly than the pressure increases thereby causing the increase in

U

dissociation with pressure. The relative importance of the different oxygen atom loss mechanisms can also be seen in Figure 12. At low pressures, wall recombination is the dominant loss mechanism. As pressure increases, the homogeneous loss terms increase with pressure cubed. At the conditions in Figure 12 the homogeneous loss terms become the same order of magnitude as the wall loss term between one and two torr. This corresponds to the maximum observed in curve 1 of Figure 8. At still higher pressures the homogeneous loss terms become more important than the wall loss terms. Reaction 3 can be neglected since it is always an order of magnitude smaller than the other homogeneous loss terms.

In comparing Figure 8 and 9 one can see that at a higher flow rate the maximum occurs at a higher pressure and the maximum is less pronounced. At low pressures conversion increases rapidly with pressure, due to the difference in magnitude in the generation and loss terms. The increase is more rapid for higher power densities due to the increase in electron density. The initial increase is greater for the lower flow rate and the greatest difference is seen at the lowest power density. The literature reports maximum conversion at lower pressures (around 0.5 torr) than the model predicts.

Figures 10 and 11 show the effect of pressure on yield for flow rates of 100 and 200 $\mu\text{mole/sec}$, respectively, for three power densities. Yield increases with pressure to a maximum and then decreases. This effect is due to the maximum seen in the conversion vs. pressure curves. Again, yield is greatest for lower power densities and higher flow rates. Experimental results in the literature show strictly an increase in yield with increasing pressure in this pressure range.

Figures 13 and 14 show the effect of power on conversion for flow rates of 50 and 200 $\mu\text{mole}/\text{sec}$, respectively, at four pressures. At all pressures and flow rates presented, conversion increases with increasing power, a trend observed experimentally^{1,2,5,6}. This is due to the increased power density, increased electron density, and, therefore, increased dissociation. For the lower flow rate (Figure 13) conversion is higher at a given power than at the higher flow rate (Figure 14).

Figures 15 and 16 show the effect of power on yield for flow rates of 50 and 200 $\mu\text{moles}/\text{sec}$, respectively, at four pressures. The yield decreases with increased power in all cases with the decrease being greatest at high pressures. Comparing Figures 15 and 16 it is seen that the yield decreases more rapidly with increasing power at the lower flow rate since relatively more oxygen atoms are generated per kilowatt hour at the higher flow rate. Bell and Kwong² report a maximum in yield with increasing power, while Mearns and Morris¹ report no change in yield with increasing power.

Figure 17 is a plot of maximum yield vs. flow rate at three power densities for a pressure of 0.67 torr. Rewriting Equation (5) as

$$-F_o N_{av}/V_p + r_o = 0$$

and considering a very large plasma volume yields

$$r_o = 0$$

which is then solved at various power densities and flow rates. The yield increases linearly with flow rate with the lower power density having the highest yield.

Figure 18 is a plot of maximum conversion vs. power. It is seen that the highest maximum conversion is at the lowest pressure and

decreases with increasing pressure. As pressure increases a larger power input is required before the asymptotic conversion is reached.

Plug Flow Model Results

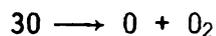
Figures 19 and 20 are plots of conversion vs. flow rate/plasma volume at power densities of 16 and 128 W/cm³, respectively, at five pressures. At both power densities conversion increases with decreasing F/V at all pressures presented. For a power density of 16 W/cm³ conversion initially increases with increasing pressure passes through a maximum and then decreases for F/V between 10⁻⁶ and 10⁻⁵. At pressures of 2.00 and 4.01 torr the conversion appears to be approaching an asymptotic value. For a power density of 128 W/cm³ conversion increases with pressure between 0.33 and 4.01 torr. Any maximum in the conversion would occur at a higher pressure and would be in excess of 90%.

Figures 21 and 22 show how yield is affected by F/V for the same conditions of power density and pressures in Figures 19 and 20. At a power density of 16 W/cm³ the yield increases with increasing F/V and with increasing pressure. For F/V between 10⁻⁶ and 10⁻⁵ the yield rises to a maximum and then decreases which is due to the maximum seen in conversion in this F/V range. For a power density of 128 W/cm³ the yield increases with F/V and pressure and no maximum is seen. With both power densities there seems to be an asymptotic value that the yield approaches. High yields are seen even at the high power densities for F/V values that are an order of magnitude larger.

CONCLUSION

A microwave plasma flow system has been designed that is capable of yielding high conversions of atomic oxygen and capable of accurately determining the oxygen atom flow rate under varied experimental conditions. The range of molecular oxygen feed rates possible is from 4 to 800 $\mu\text{mole}/\text{sec}$; pressures can be varied from 0.5 to a few hundred torr, keeping flow rate constant. Power can be varied continuously from near zero to 1400 watts. Preliminary experiments have yielded conversions of 4.0 and 9.3% for oxygen flow rates of 66.4 and 51.8 $\mu\text{moles}/\text{sec}$, respectively, at the relatively high pressure of 3.4 torr.

Plug flow and CSTR models of atomic oxygen generation in a plasma have been developed that include the electron impact dissociation reaction, three homogeneous gas phase recombinations reactions, and a heterogeneous wall recombination reaction. Results show that the reaction



can be neglected in the pressure range studied (0.33 to 4.01 torr) and at a neutral gas temperature of 298°K, since the other gas phase recombination reactions are an order of magnitude greater.

The models are based on current literature estimates of electron density and the rate constant for electron impact dissociation of molecular oxygen under varying conditions of power density and pressure. Both models predict the decrease in conversion and increase in yield with decreasing flow rate that has been observed experimentally. Both models predict a maximum in conversion and yield as pressure increases that depends on power density and flow rate, with the maximum occurring at higher pressures, the higher the flow rate and power density is.

Experimental results from the literature indicate maxima at lower pressures and more rapid decreases in conversion with increasing pressure than the model predicts. This suggests that more work needs to be done in how electron density and the rate constants for electron impact dissociation of diatomic gases change with discharge parameters such as pressure and power density. Work also needs to be done in determining wall recombination coefficients for oxygen as a function of temperature since many discrepancies in these values exist in the literature and wall recombination is the dominant loss mechanism for atomic oxygen at low pressures. Both models predict the experimentally observed effects of increasing conversion and decreasing yield upon increasing power density with results that are very near literature values.

Both models developed are based on a neutral gas temperature of 298°K in the discharge. Actual temperatures are no doubt much higher, possibly as high as 800°K. Since all rate constants are temperature dependent, the conversions and yields predicted are higher than would be predicted by using a gas temperature of 800°K. However, the models do shed light on what factors are important in both modeling plasma systems and designing and performing experiments.

FUTURE WORK

A system has been designed and tested for the production of oxygen atoms and their detection. Experiments should be performed to verify the data obtained by earlier investigators using conditions as close as possible to the experimental conditions described. Once this benchmark has been made, experiments can be performed using higher power densities than previously reported to determine what the upper limit on conversion is under varying conditions. The annular discharge tubes designed and built should be experimentally tested to determine if higher conversions are possible or if excessive wall recombinations occur due to the larger surface area available for recombination. An analysis of the electric field in cylindrical flow needs to be done so that a more accurate determination of electron density and the rate constant for electron impact dissociation as a function of power density and pressure can be made, and then used in modeling of the plasma in both cylindrical and annular flow situations. Finally, an energy balance on the entire plasma system should be done so that the microwave losses to the cavity wall can be determined and so that the overall energetics of oxygen atom production can be studied.

Table 1 Summary of Oxygen Atom Generation Studies

Worker	Bell and Kuo ²	Hearns and Morris ¹	Batley ⁴	Brown ³
Experimental Conditions				
Pressure (torr)	2.00	2.00	1.00	0.52
Neutral Gas Temp. (°K)	2.00	300	0.50	0.52
Gas Flow Rate (gmole/sec)	1.4x10 ⁻⁵	1.92x10 ⁻⁴	6.13x10 ⁻⁴	1.8x10 ⁻⁵
Power Absorbed (watts)	73	208	100	4.77x10 ⁻⁷
				0 ₂ : 1.8x10 ⁻⁵
				H ₂ O: 4.77x10 ⁻⁷
				20
				20
Dimensions				
Inside Diameter (mm)	8 cm dia. x 2.5 cm high	21.8	10.6	10
Length (cm)	---	---	---	---
Plasma Volume (cm ³)	---	70	2.5	---
Area/Volume (cm ⁻¹)	---	0.0633	0.3530	---
Coating	none	none	none	none
Discharge Characteristics				
Frequency (Mhz)	13.56	2450	13.56	2450
Power Density (watts/cm ²)	0.5809*	2.97	.0093*	---
Electron Density (electrons/cm ³)	2.17x10 ¹⁰	7.13x10 ¹⁰	---	---
Electron Temperature (°K)	4000	0.90	---	---
P/A (torr cm)	1.59	14	4.22	0.11
E/p (Volt/cm Torr)	12	14	---	27.5
Plasma Residence Time (nsec)	---	49	---	1.0-4.0
Conversion (%)				
Yield (gmole/tonh)	12	15	3.2	28
Flow Rate for 1 lbf thrust (gmole/sec)	0.15	0.72	1.40	1.81
Scale Factor (1bf thrust Flow) (exp. Flow)	0.0725	0.0683	0.1410	0.0474
	5176	4482	230	2635
			340	2762

*based on total reactor volume -- not plasma volume

TABLE 2

Rate Coefficients for Neutral Collision Partners in O₂ Dissociation*

<u>Reaction No.</u>	<u>Reaction</u>	<u>Rate Coefficient</u>	<u>Reference</u>	
1	O + O ₃ → 2O ₂	6.6x10 ⁻¹⁵	9	
		1.1x10 ⁻¹⁴	10	
		3.9x10 ⁻¹⁵	11	
		2x10 ⁻¹⁴	12	
		9x10 ⁻¹⁵	13	
2	O + O + O → O ₂ + O	3.8x10 ⁻³³	33(35)	
		3.6x10 ⁻³³	34	
3	O + O + O ₂ → O ₂ + O ₂	1.2x10 ⁻³³	34(35)	
		4.4x10 ⁻³⁴	33(35)	
		2.3x10 ⁻³³	36(35)	
		2.5x10 ⁻³³	37(35)	
		6.3x10 ⁻³⁴	38(35)	
		1.4x10 ⁻³⁴	39(35)	
		3.0x10 ⁻³³	40	
4	O + O ₂ + O ₂ → O ₃ + O ₂	2.8x10 ⁻³⁴	25	
		3.7x10 ⁻³⁴	11	
		7.5x10 ⁻³⁴	41,42	
		6.5x10 ⁻³⁴	43	
		(298°K) 8.8x10 ⁻³⁴	44	
5	O + O ₂ + O ₃ → O ₃ + O ₃	8.0x10 ⁻³⁴	45,11(35)	
		8.8x10 ⁻³⁴	46(35)	
		3.6x10 ⁻³⁴	11	
6	NO + O + M → NO ₂ + M	M=Ar, O ₂	7.6x10 ⁻³²	47
		M=N ₂	5.0x10 ⁻³²	48
		M=N ₂	1.03x10 ⁻³²	49
		M=N ₂ (297°K)	1.26x10 ⁻³¹	50
		M=O ₂	5.5x10 ⁻³¹	51
		M=O ₂	8.0x10 ⁻³²	52
		M=O ₂ , Ar, He	5.1x10 ⁻³²	53
		M=Ar	3.7x10 ⁻³²	54
M=CO ₂ (293°K)	5.5x10 ⁻³²	53		
7	NO ₂ + O → NO + O ₂	3.5x10 ⁻¹²	48	
		1.6x10 ⁻¹²	50	
		5.5x10 ⁻¹²	49	
		2.49x10 ⁻¹²	12	
8	NO + O → NO ₂ + hν	1x10 ⁻¹⁷	55	

TABLE 2 (cont.)

<u>Reaction No.</u>	<u>Reaction</u>		<u>Rate Coefficient</u>	<u>Reference</u>
9	$O + O_2 + M \rightarrow O_3 + M$	M=Ar	5.0×10^{-34}	56
		M=Ar	7.8×10^{-34}	44
		M=Ar(296°K)	2.3×10^{-34}	42
		M=Ar	4.0×10^{-34}	43
		M=CO ₂	2.6×10^{-33}	44
		M=CO ₂	1.5×10^{-33}	43
		M=He(298°K)	6.3×10^{-34}	44
		M=He	4.0×10^{-34}	43
		M=N ₂	5.6×10^{-34}	43
		M=N ₂ O	15×10^{-34}	43
M=H ₂ O	60×10^{-34}	43		
10	$O + O \rightarrow 2O$		3.9×10^{-15}	11
			9.0×10^{-15}	56
			6.5×10^{-15}	57
11	$O + O + N_2 \rightarrow O_2 + N_2$		2.9×10^{-33}	58
12	$CO + O_2 + O \rightarrow CO_2 + O_2$		7.8×10^{-31}	40
13	$C + O_2 + O \rightarrow CO + O_2$		4.8×10^{-33}	40
14	$O + H_2O \rightarrow OH + O_2$		3.6×10^{-11}	59
15	$O + OH \rightarrow H + O_2$		4.0×10^{-11}	60
16	$O + H_2 \rightarrow OH + H$		2.46×10^{-18}	61
			2.83×10^{-18}	60
			2.64×10^{-18}	62

*Additional rate coefficients for reactions of uncharged species can be found in references 14 to 31. Rate coefficients for reactions of charged species can be found in references 70 to 75.

TABLE 3
Surface Recombination Coefficient of Oxygen Atoms at 20°C

<u>Material</u>	<u>Probability of Recombination</u>	<u>Ref.</u>
Mg	2.6×10^{-3}	79,80
Au	5.2×10^{-3}	79,80
Ni	2.8×10^{-2}	79,80
Fe	3.6×10^{-2}	79,80
Cu	1.7×10^{-1}	79,80
Ag	2.4×10^{-1}	79,80
NaCl	9.4×10^{-4}	79,80
Pyrex	3.1×10^{-5} - 1.2×10^{-4} $(.4-.68) \times 10^{-5}$	79,80,82 83
Silica	$(.17-1.6) \times 10^{-4}$	79,80,45,82
Quartz	$(.4-.8) \times 10^{-4}$	83

TABLE 4
Summary of Preliminary Experiments

Design	Discharge Pressure (torr)	Power Absorbed (watts)	O ₂ Flow Rate (μmole/sec)	Conversion (%)
a	1.7	1323	251.9	0.28
a	2.3	1323	251.9	0.14
a	3.3	1323	251.9	0.08
a	2.3	1323	509.3	0.34
a	0.5	1400	38.4	0.35
a	0.5	1361	70.8	0.18
a	2.3	1281	407.1	0.34
a	3.3	1281	407.1	0.17
b	1.0	1337	151.5	1.11
b	1.0	1342	108.6	1.50
b	1.0	1342	82.9	1.64
b	1.0	1342	53.1	1.29
b	1.0	1342	44.0	1.34
b	0.5	1342	53.1	1.52
c	3.5	1330	66.4	4.00
c	3.4	1400	51.8	9.30

- a 28 mm ID tube, aluminum connections, sparger injectors, 2 inch downstream pipe
- b 0.8 mm ID tube, ground quartz connections, sparger injectors, 2 inch downstream pipe
- c 0.8 mm ID tube, ground quartz connections, pepperpot injectors, 1 inch downstream pipe

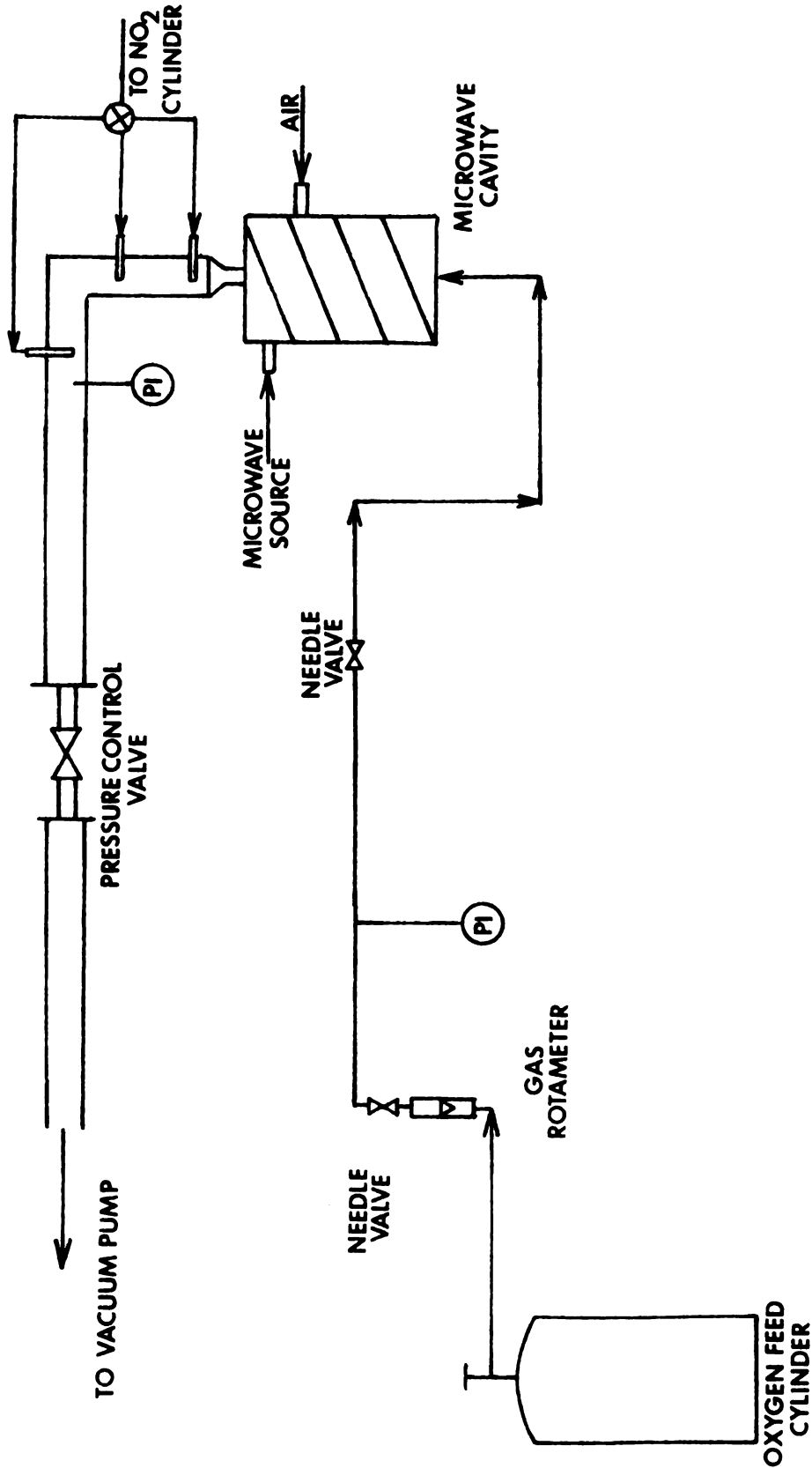


Figure 1 Microwave Plasma Flow System

U

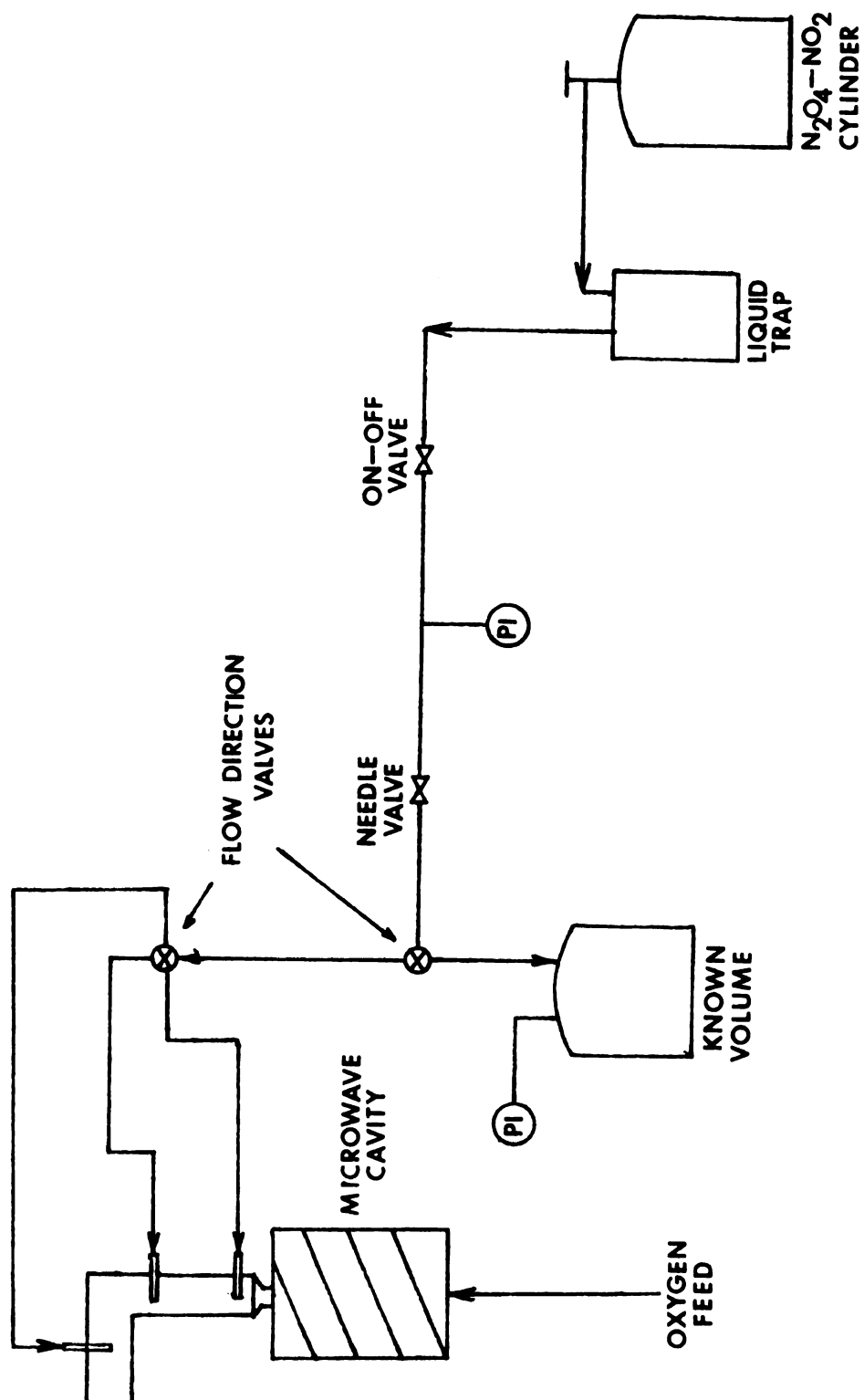


Figure 2 NO_2 Titration Flow System

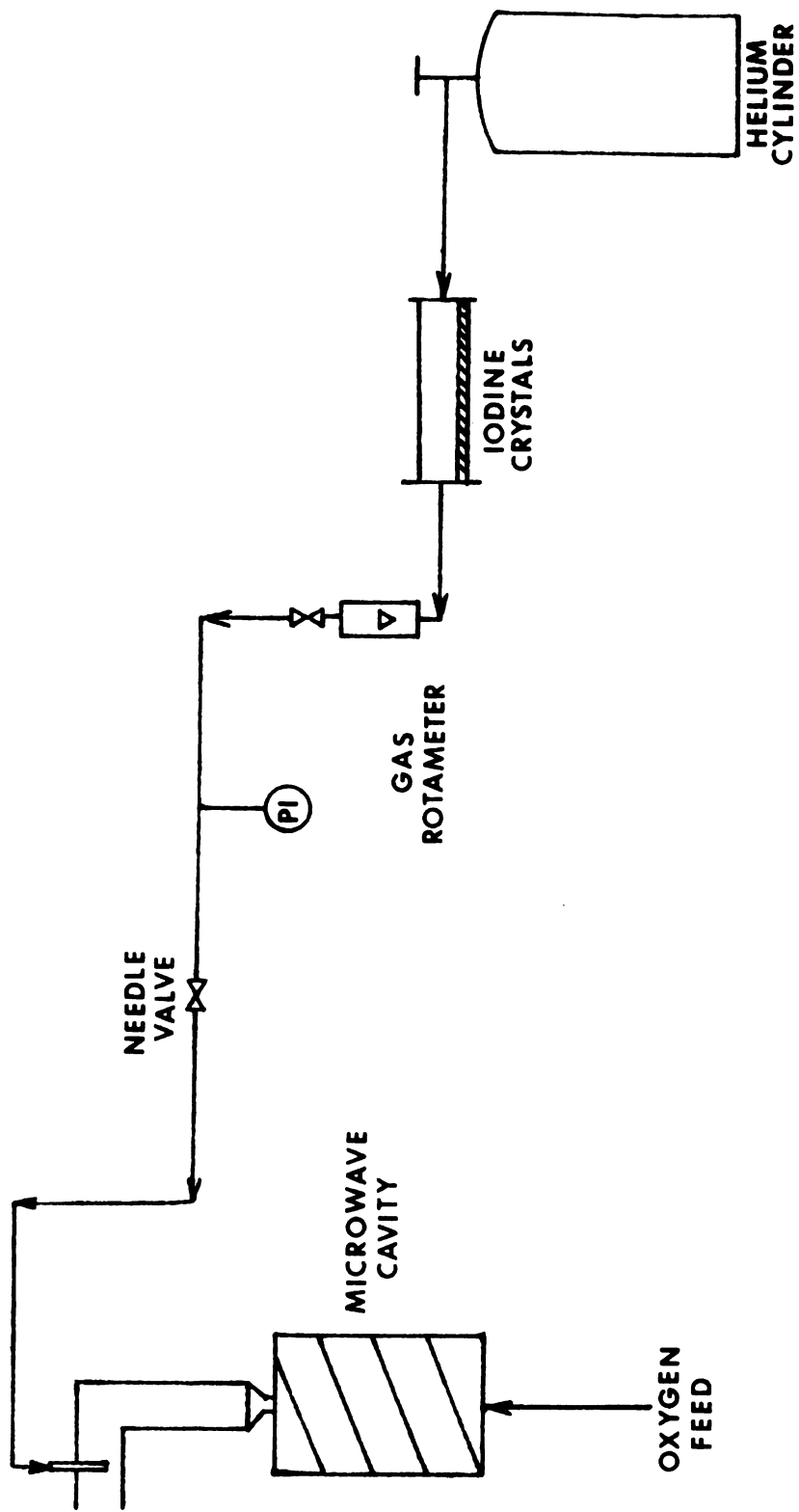


Figure 3 $1\Delta_g(O_2)$ Detection System

FIGURE 4 CONVERSION vs FLOWRATE CSTR MODEL

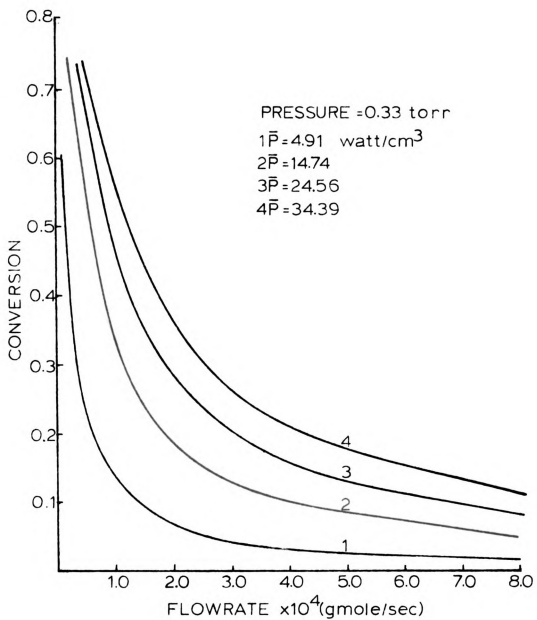


FIGURE 5 CONVERSION vs FLOWRATE CSTR MODEL

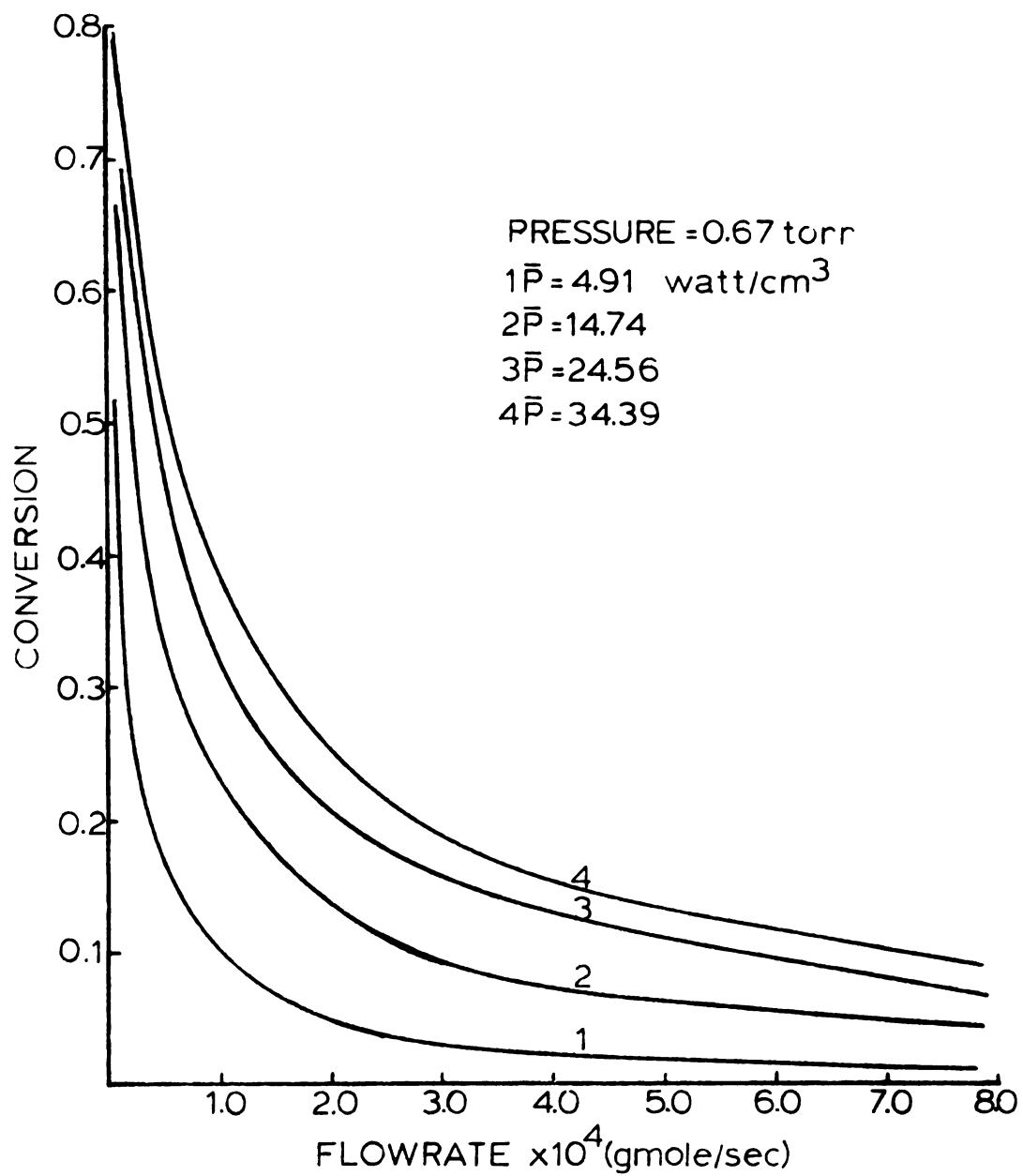


FIGURE 6 YIELD vs FLOWRATE CSTR MODEL

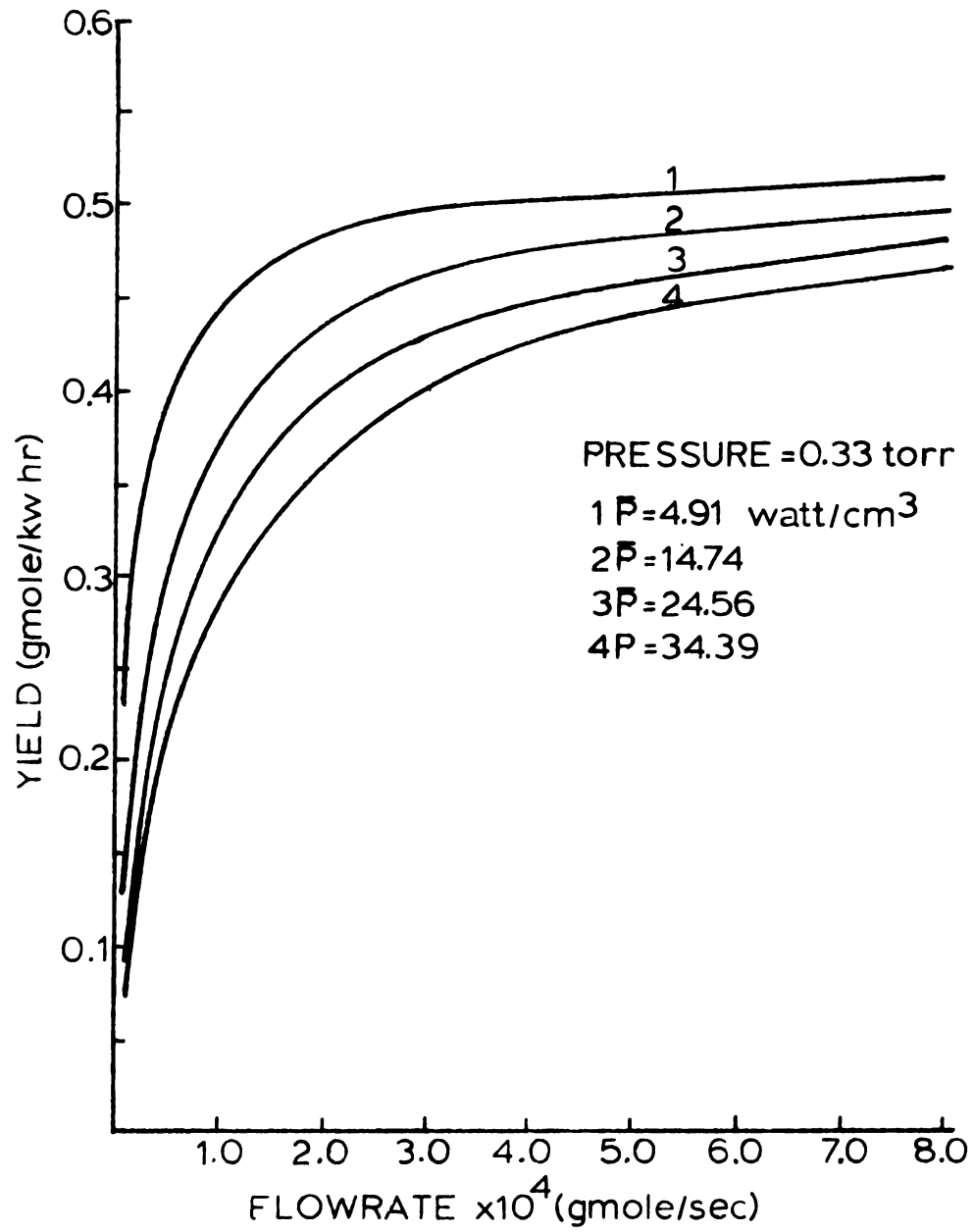


FIGURE 7 YIELD vs FLOWRATE CSTR MODEL

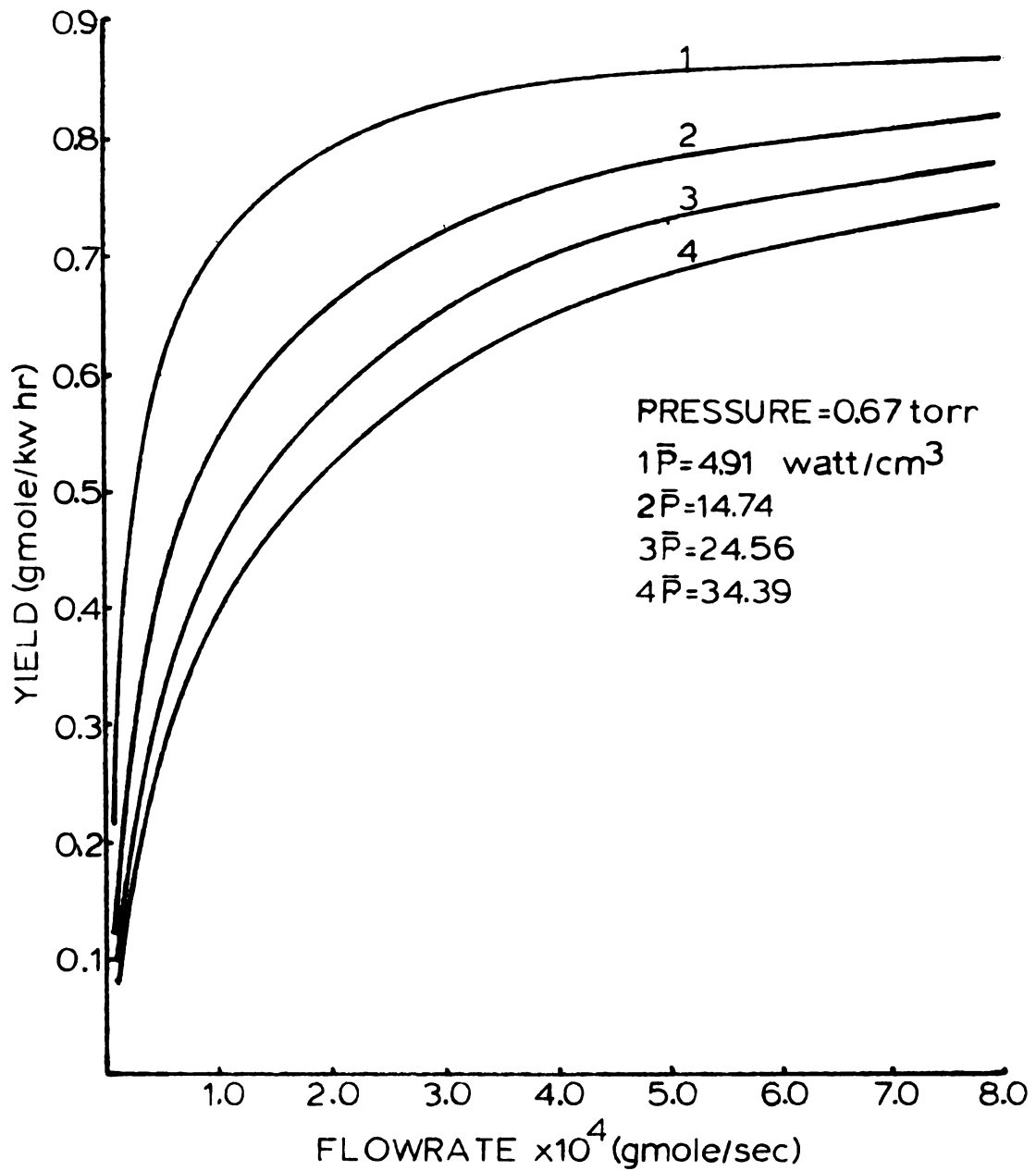


FIGURE 8 CONVERSION vs PRESSURE CSTR MODEL

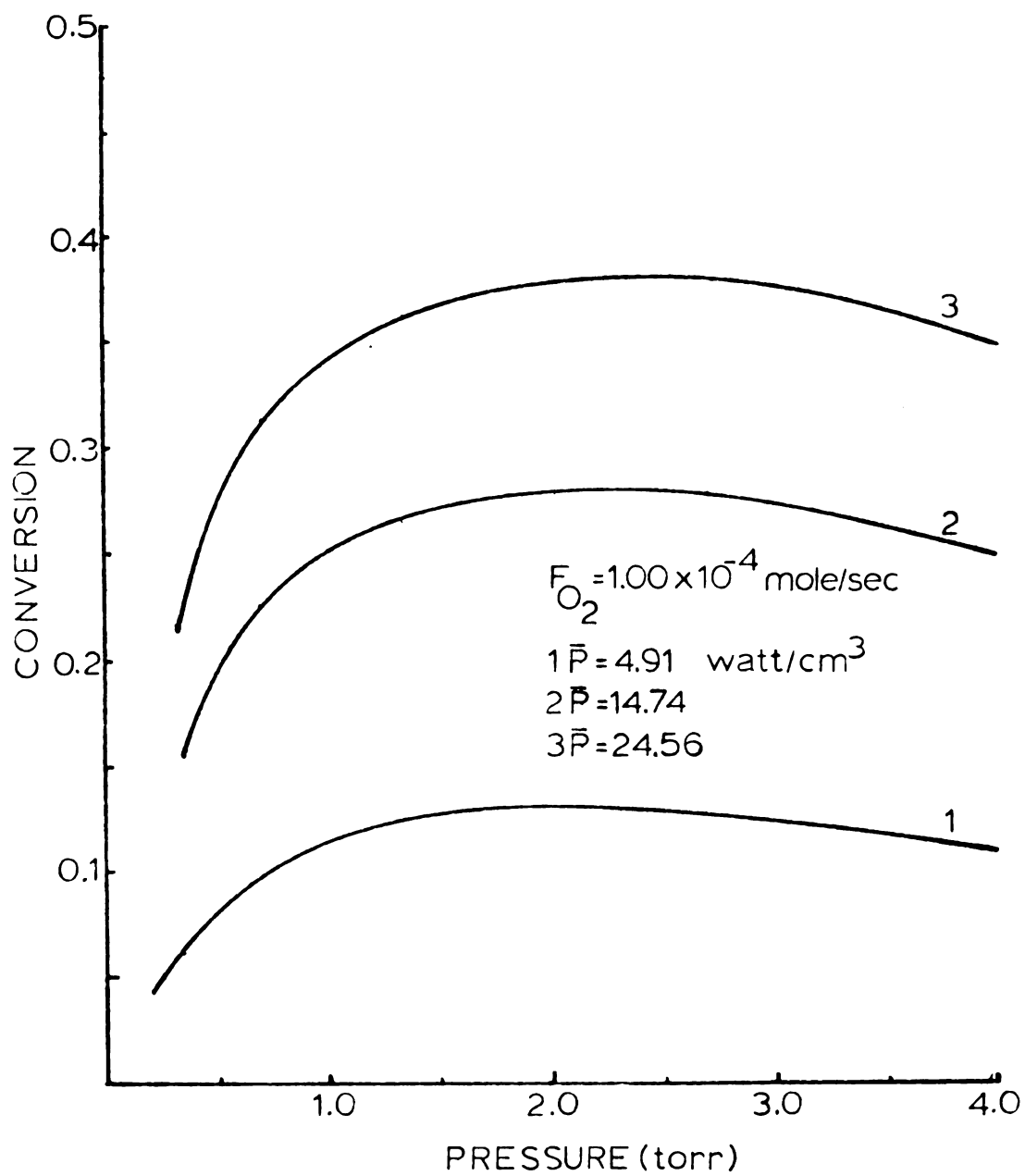


FIGURE 9 CONVERSION vs PRESSURE CSTR MODEL

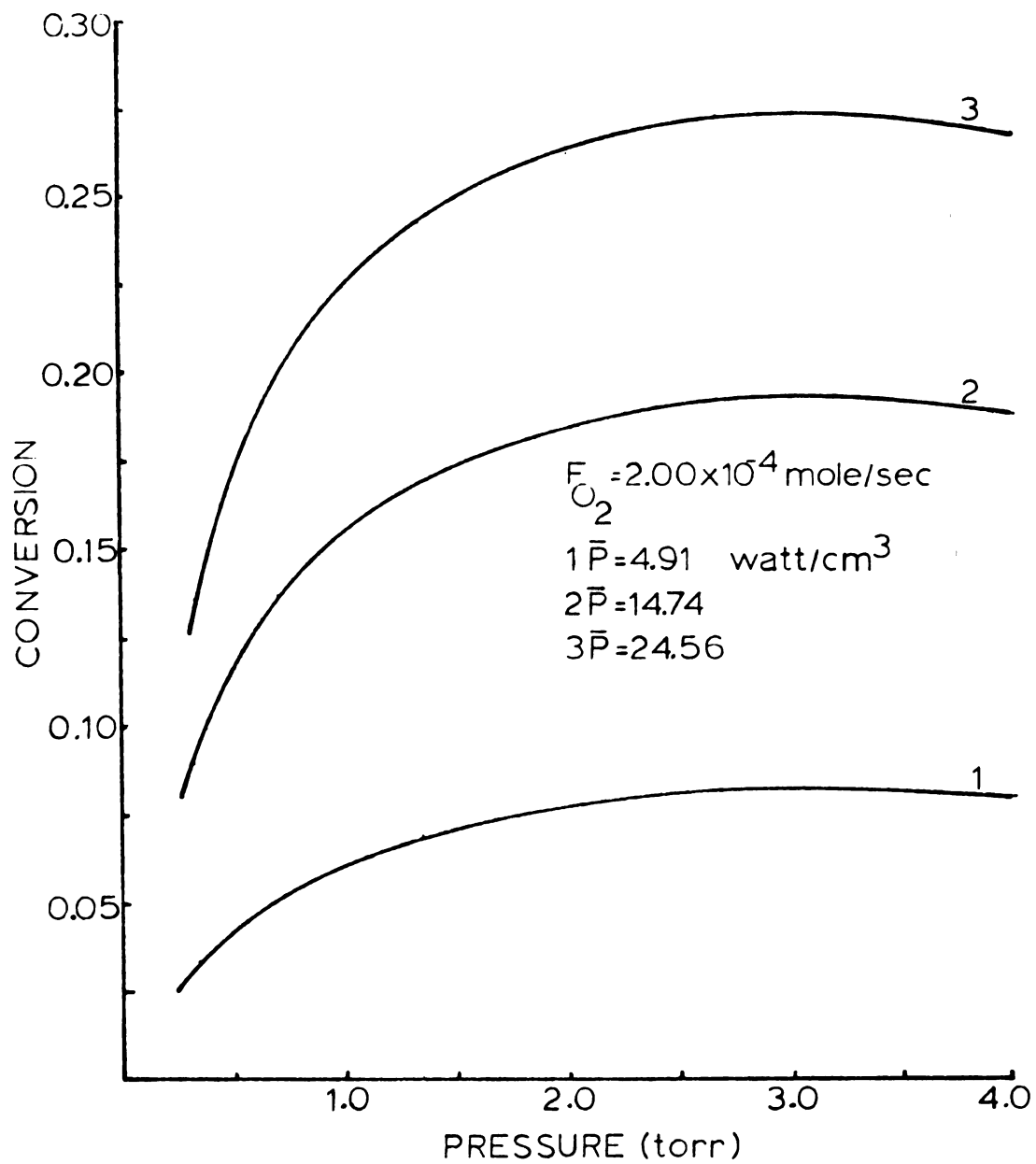


FIGURE 10 YIELD vs PRESSURE CSTR MODEL

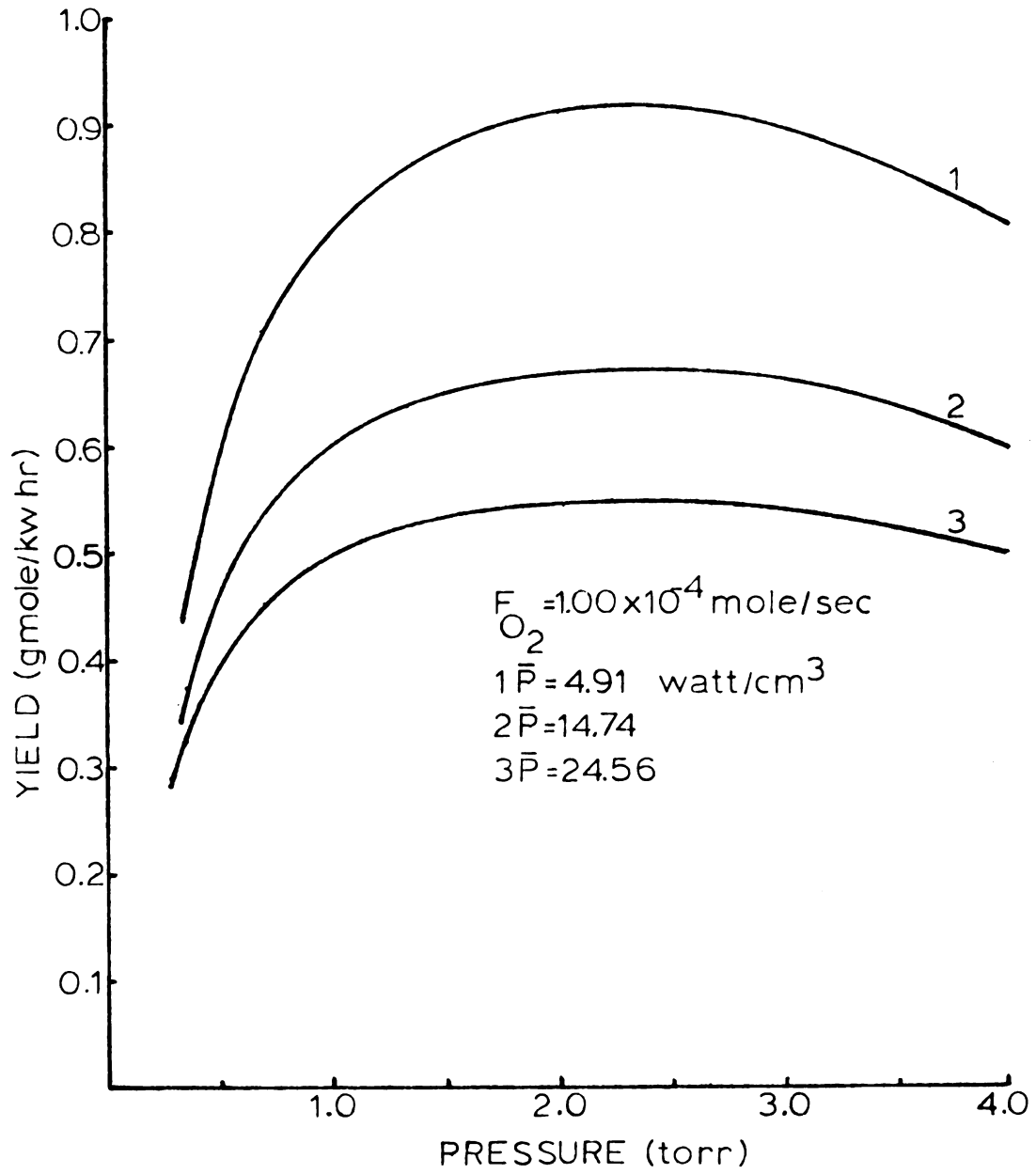


FIGURE 11 YIELD vs PRESSURE CSTR MODEL

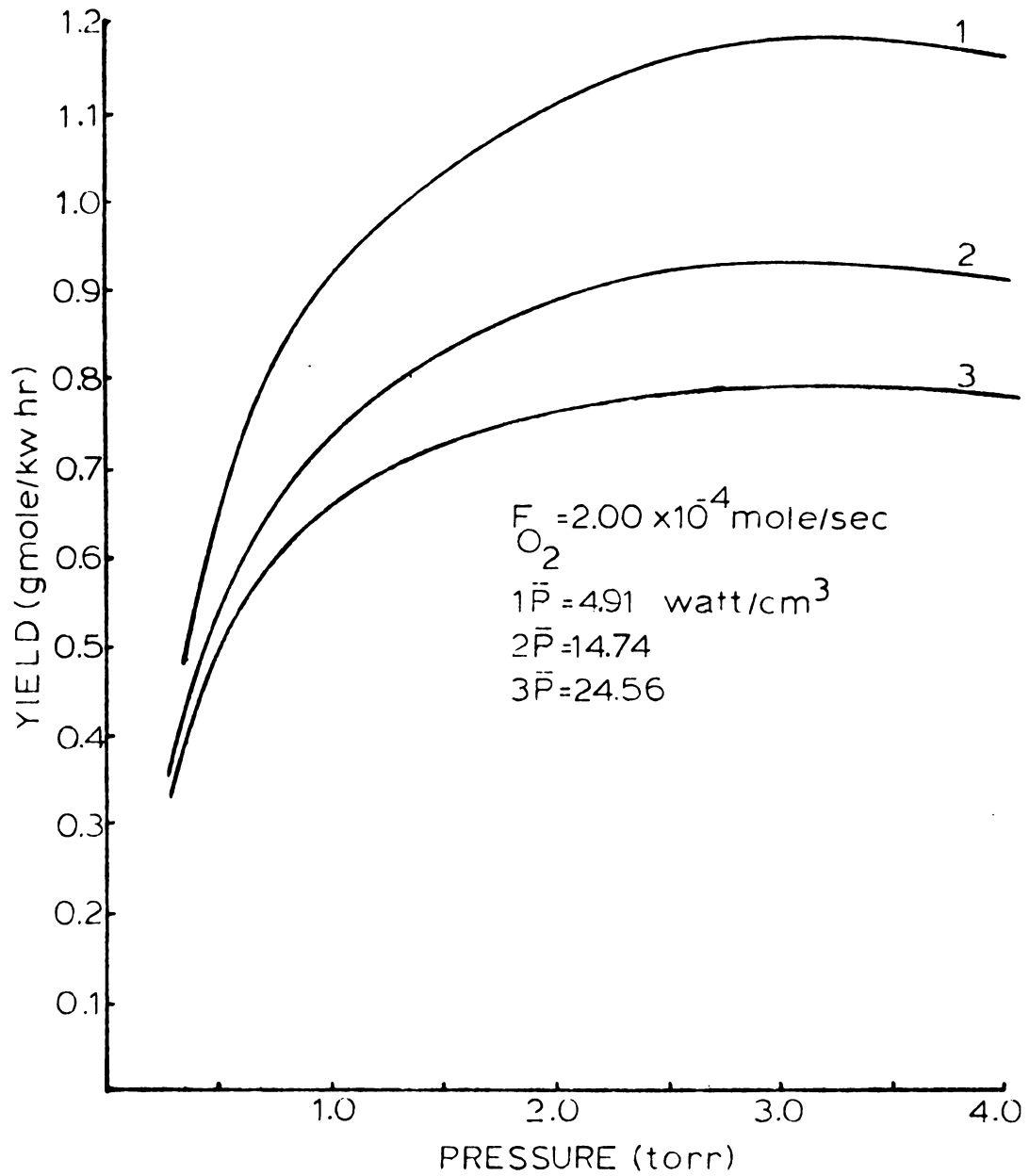


FIGURE 12 EFFECT OF PRESSURE ON CSTR MODEL TERMS

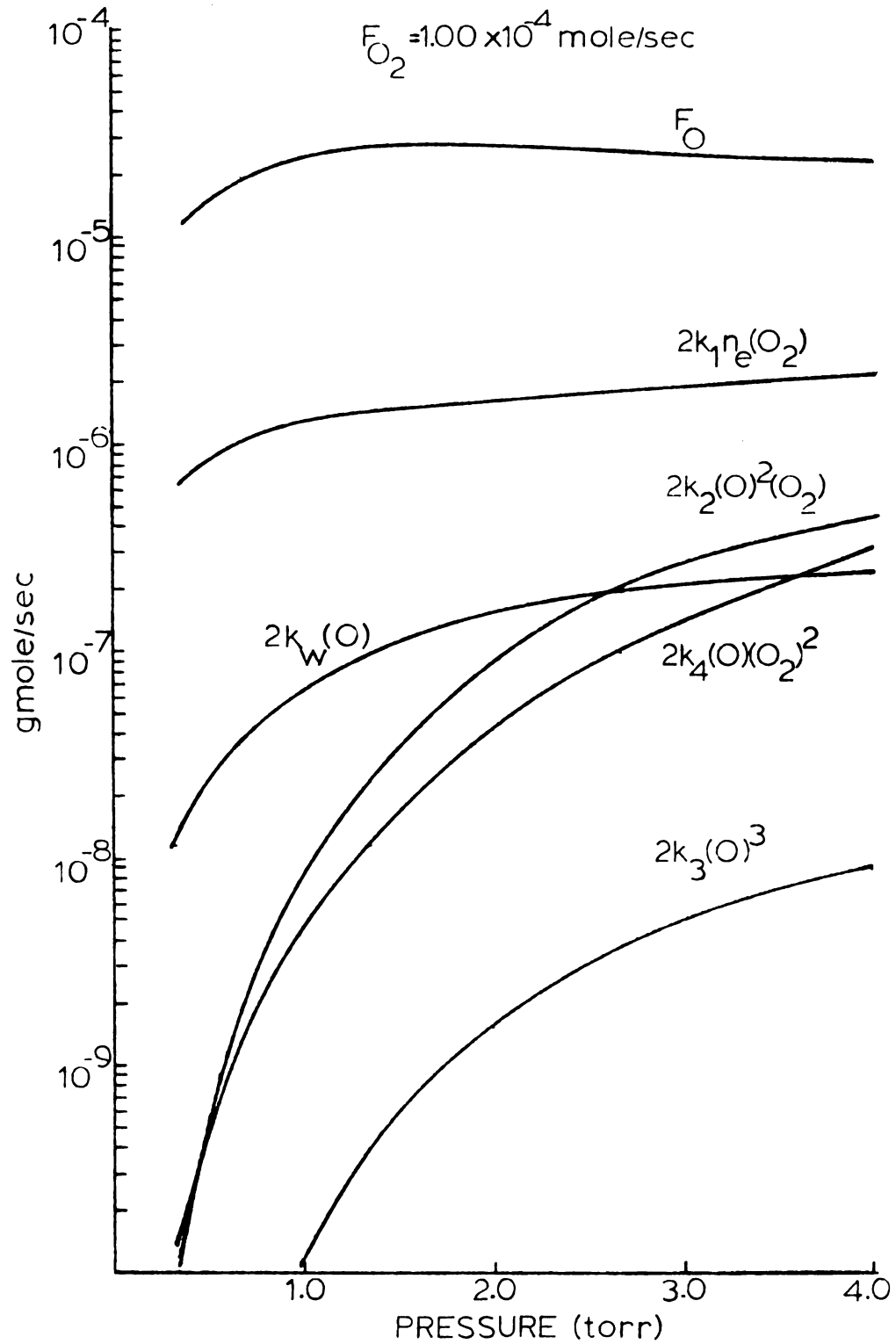


FIGURE 13 CONVERSION vs POWER CSTR MODEL

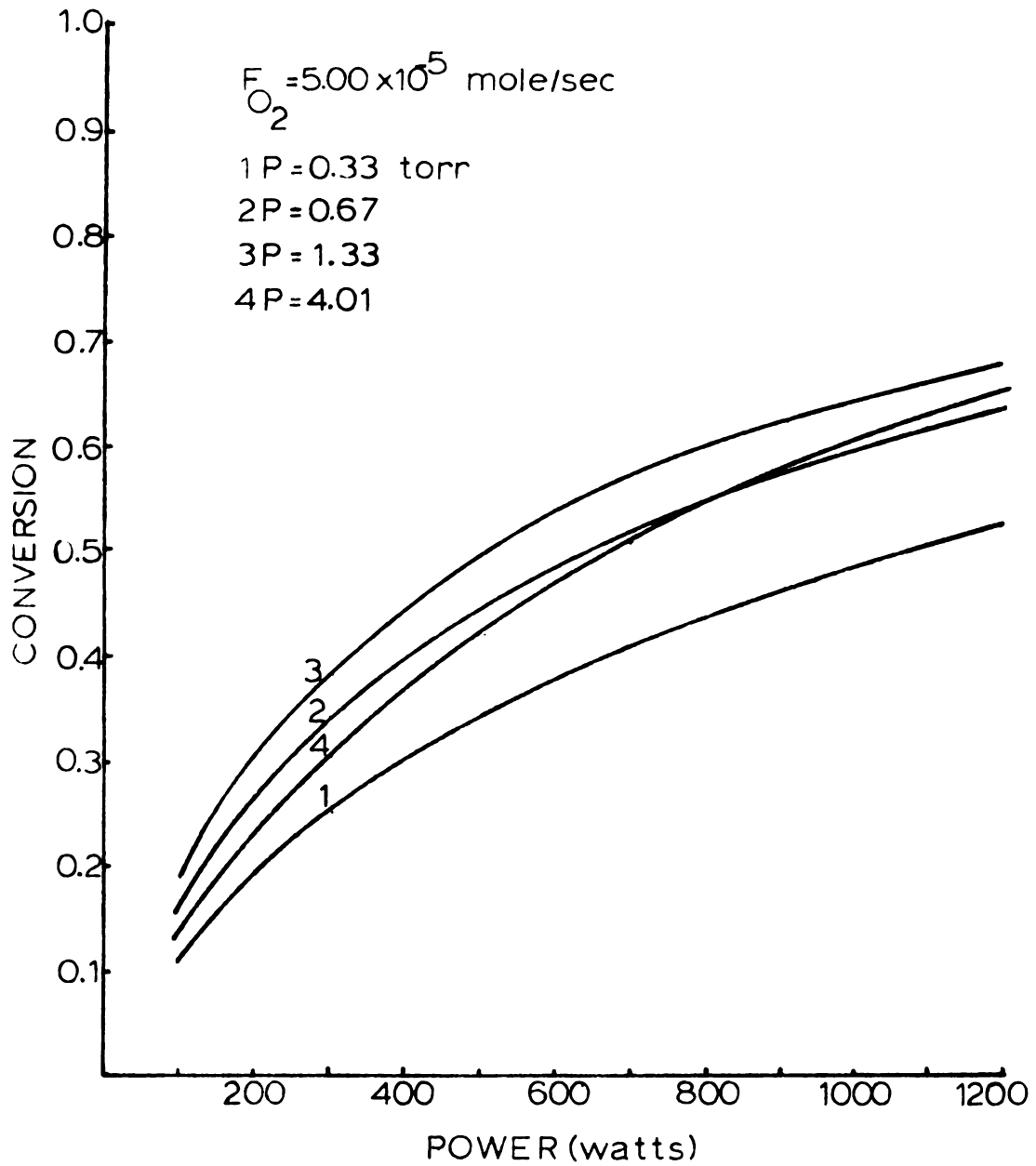


FIGURE 14 CONVERSION vs POWER CSTR MODEL

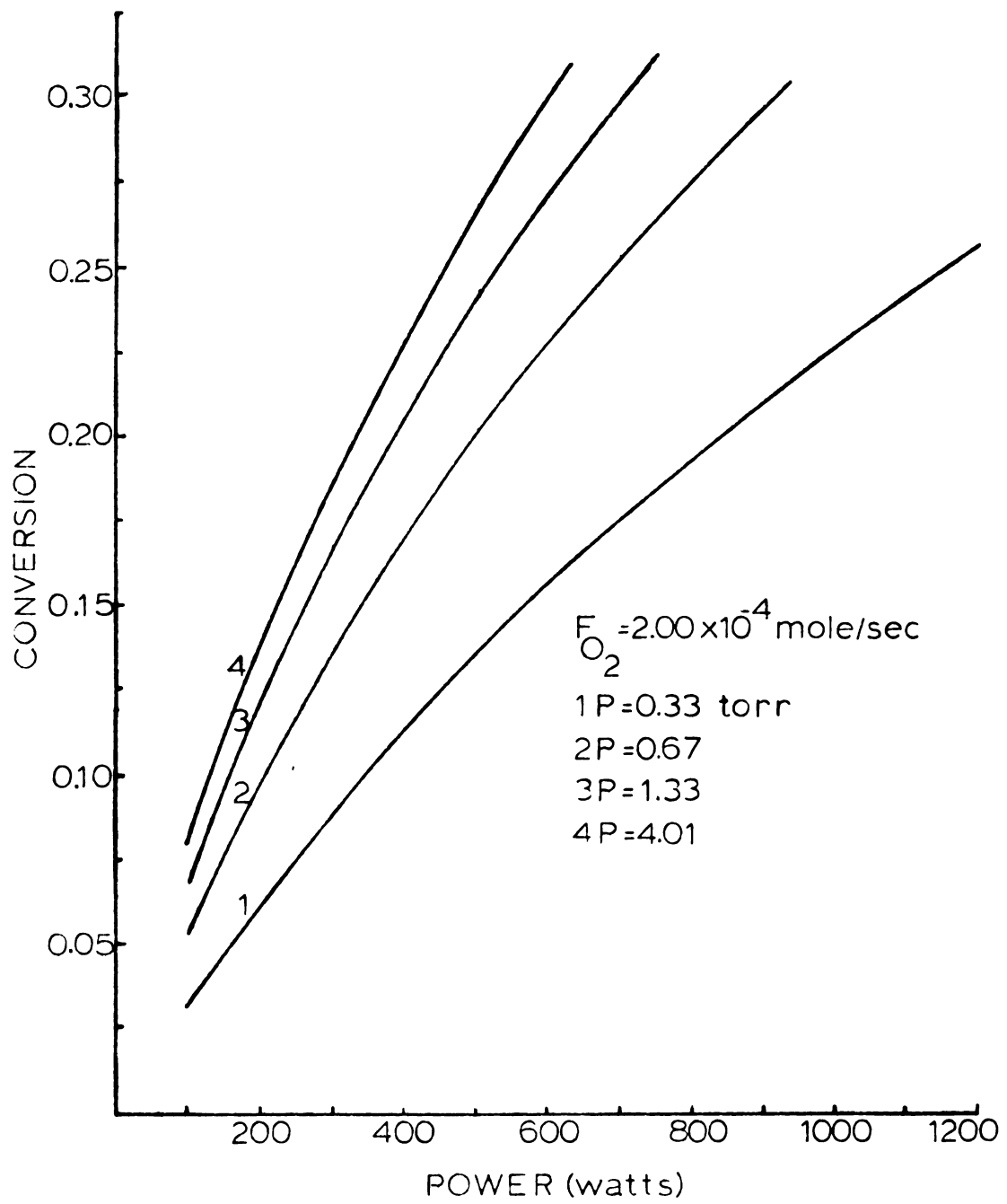


FIGURE 15 YIELD vs POWER CSTR MODEL

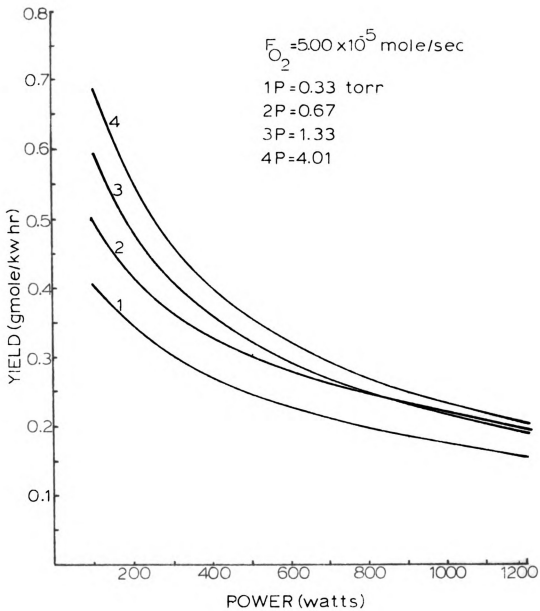


FIGURE 16 YIELD vs POWER CSTR MODEL

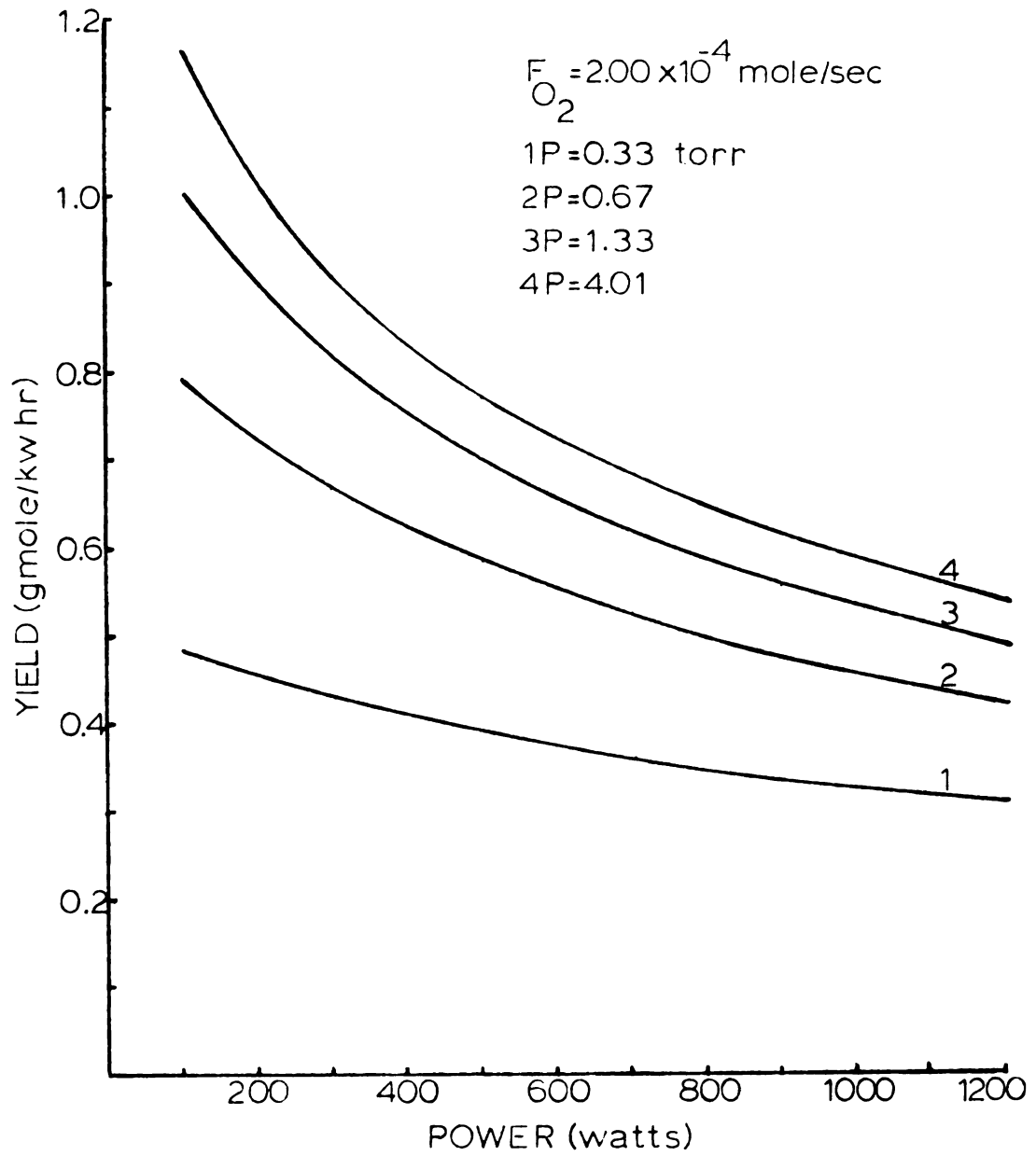


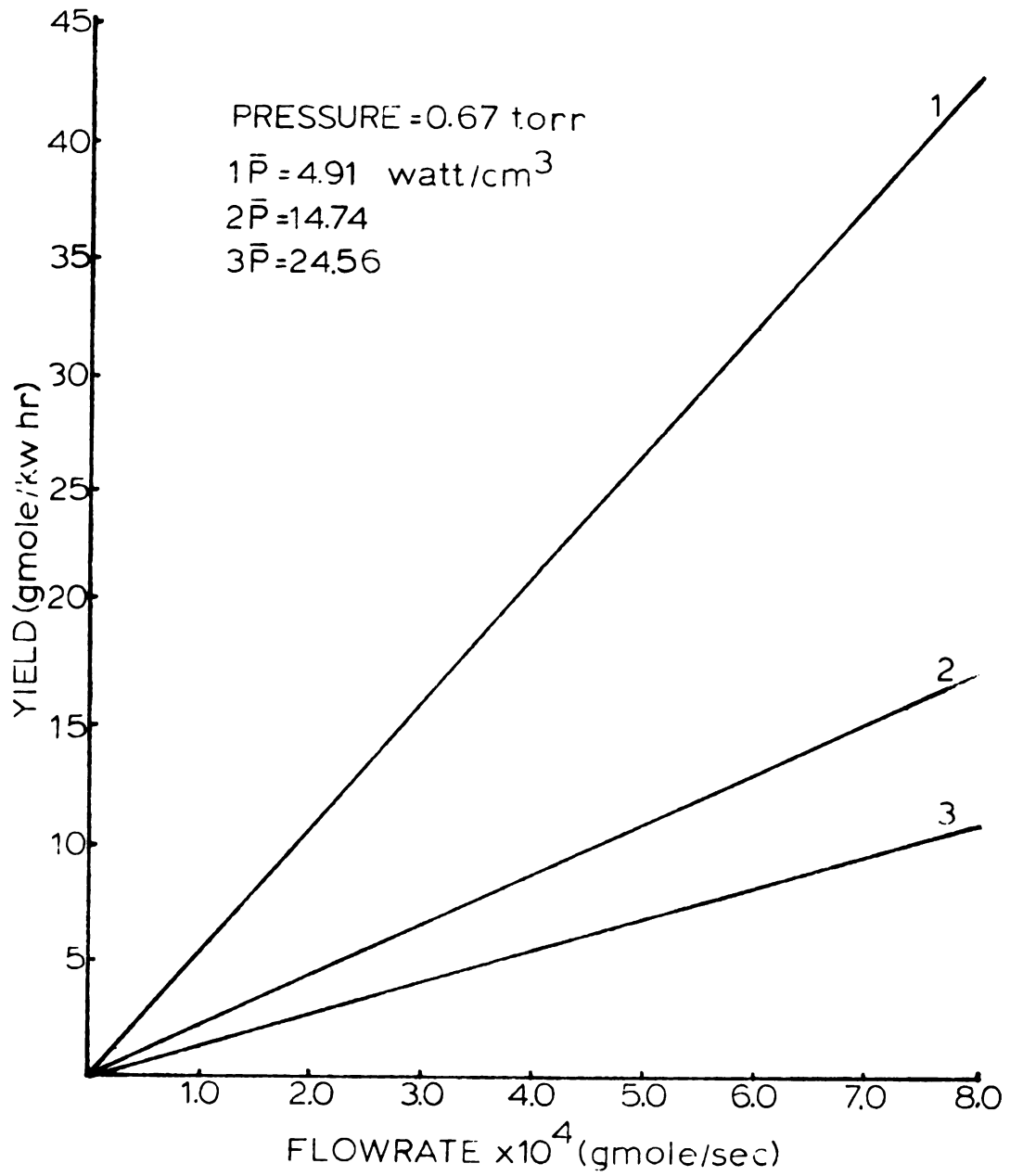
FIGURE 17 MAXIMUM YIELD vs FLOWRATE
CSTR MODEL



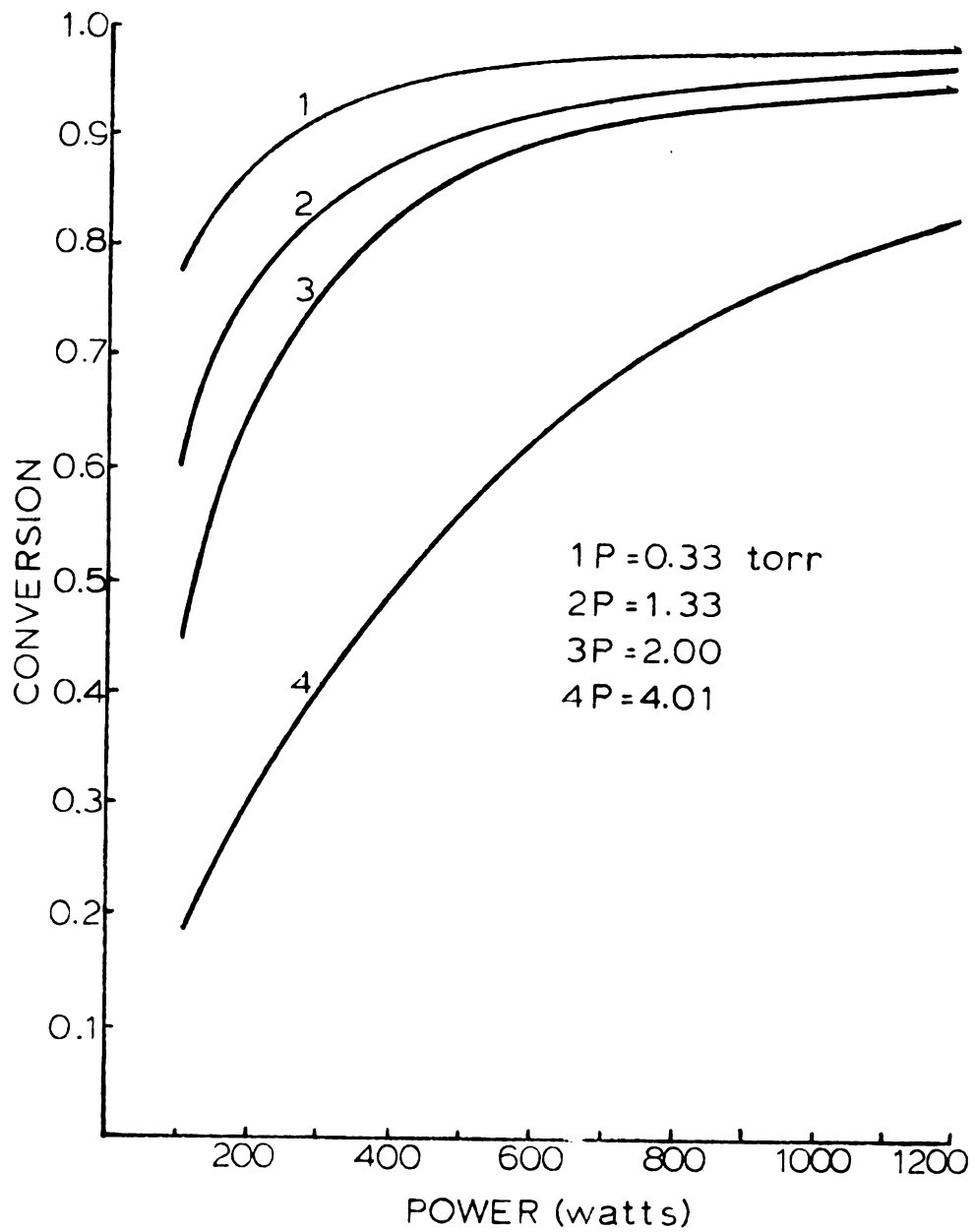
FIGURE 18 MAXIMUM CONVERSION vs POWER
CSTR MODEL

FIGURE 19 CONVERSION vs F/V PLUG FLOW MODEL

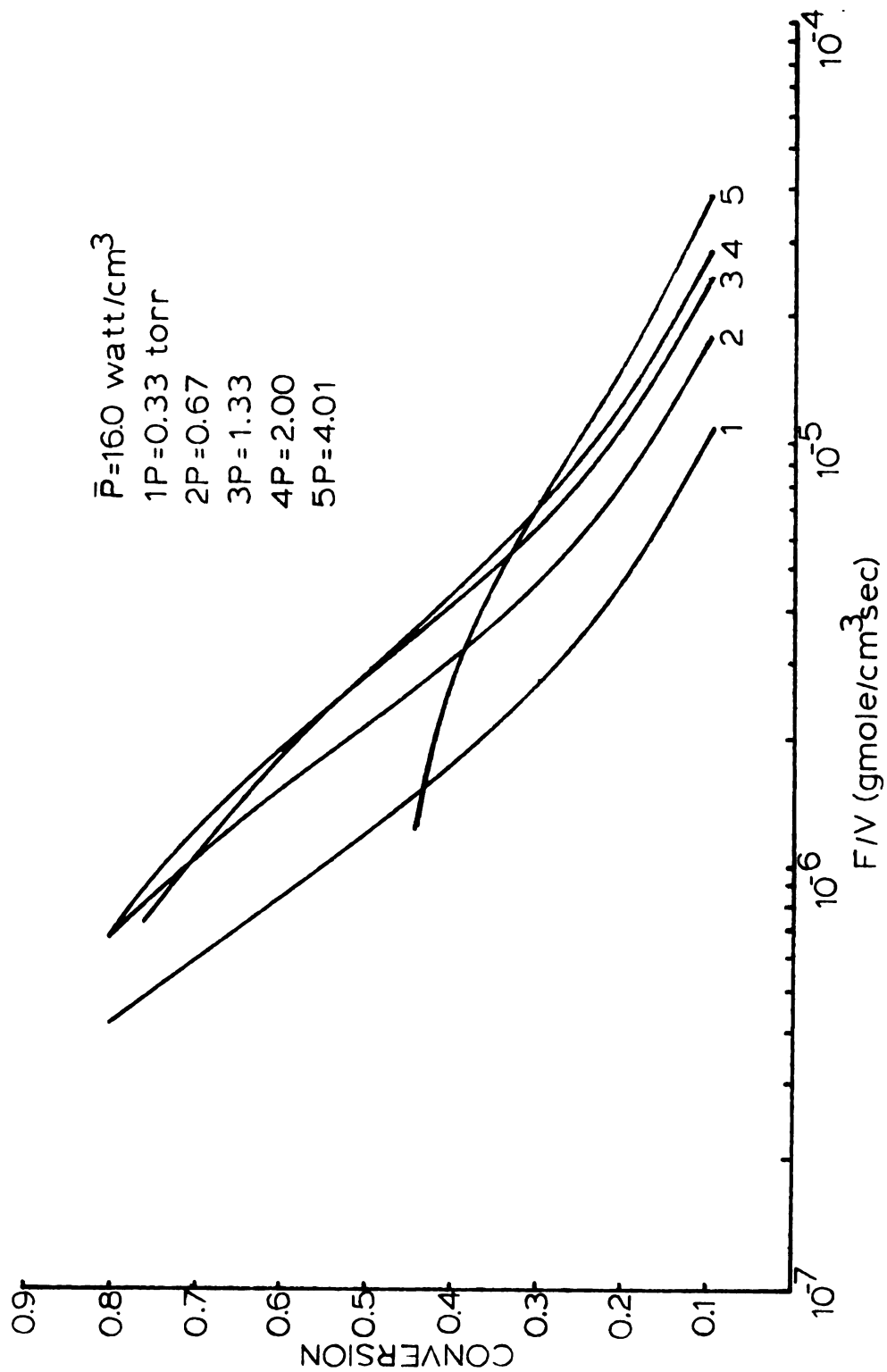


FIGURE 20 CONVERSION vs F/V PLUG FLOW MODEL

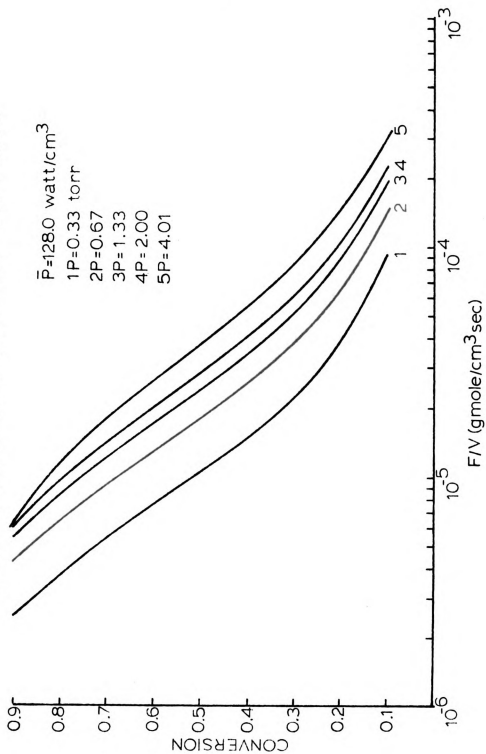


FIGURE 21 YIELD vs F/V PLUG FLOW MODEL

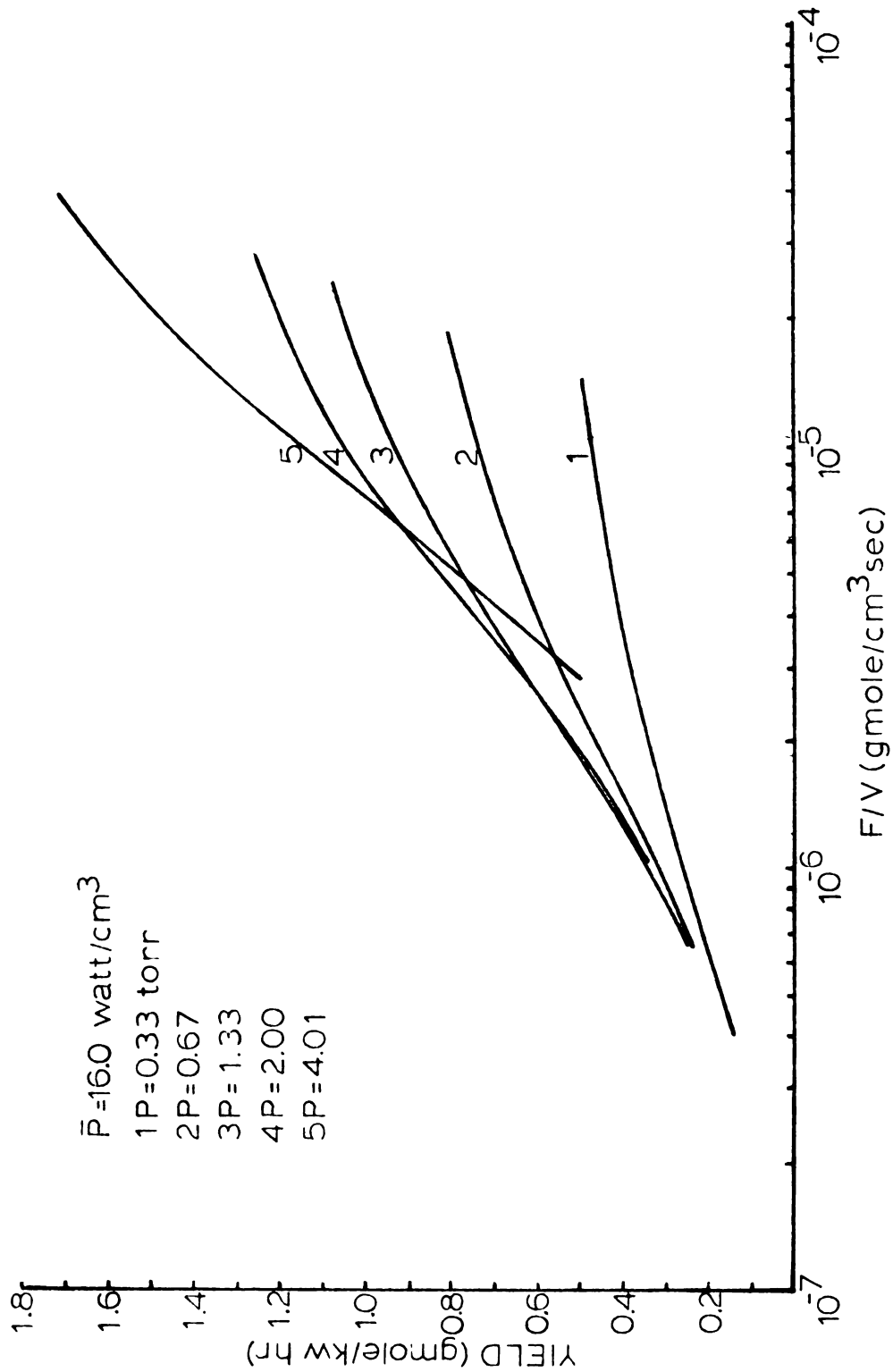
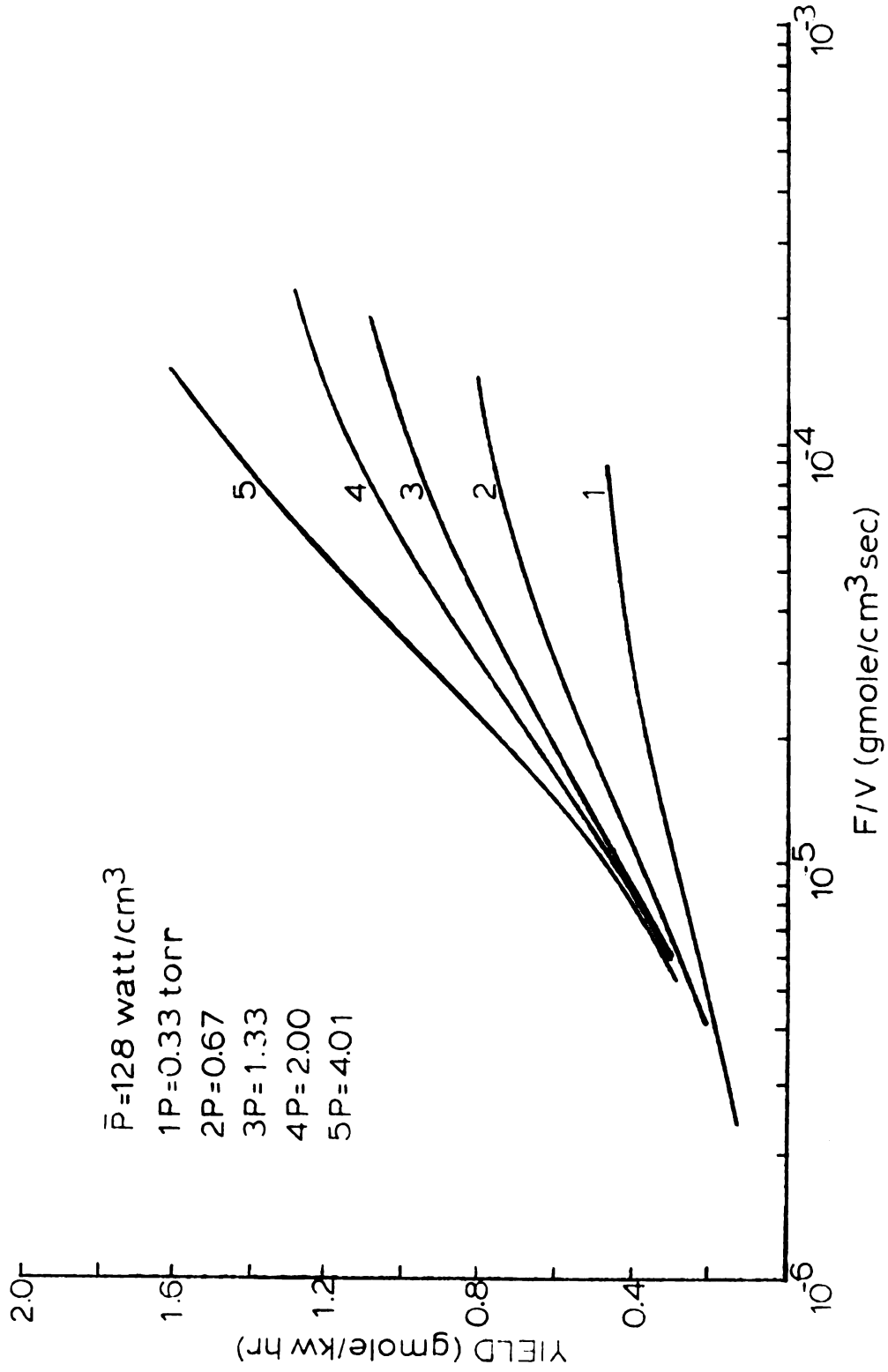


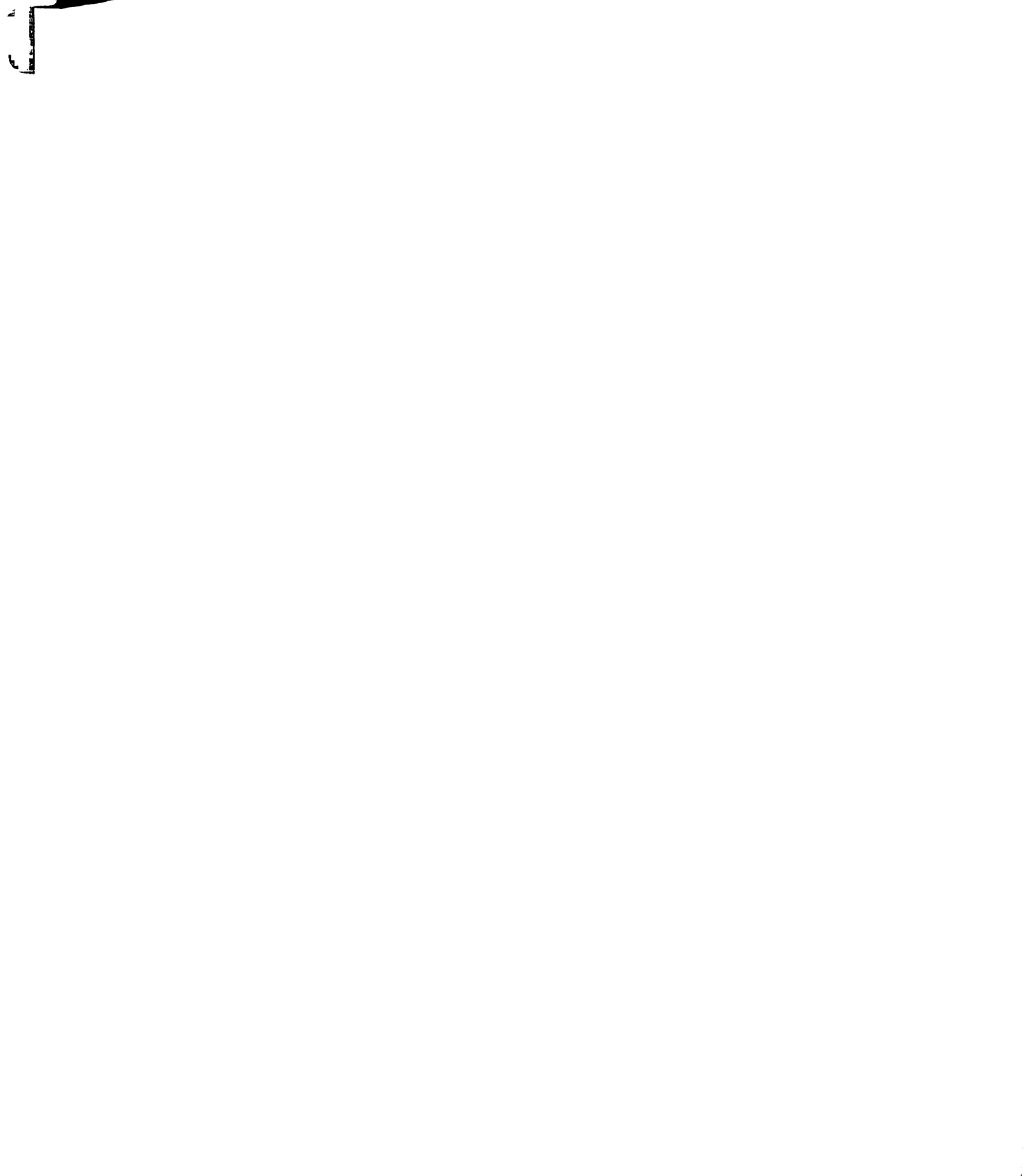
FIGURE 22 YIELD vs F/V PLUG FLOW MODEL



REFERENCES

1. Mearns, A. M., and Morris, A. J., CEP Symp. Ser. 67, No. 112, 37 (1971).
2. Bell, A. T., and Kwong, K., AIChE J. 18, 990 (1972).
3. Brown, R. L., J. Phys. Chem. 71, 2492 (1967).
4. Battey, J. F., IEEE Trans. Elect. Dev., Ed. 24, 140 (1977).
5. Bell, A. T., CEP Symp. Ser 67, No. 112, 1 (1971).
6. Bell, A. T., and Kwong, K., Ind. Eng. Chem. Fundam. 12, 90 (1973).
7. Kaufman, F., Adv. Chem. Ser. 80, 29.
8. Hake, R. D., and Phelps, A. V., Phys. Rev. 158, 70 (1967).
9. Clark, I. D., Jones, I. T. N., and Wayne, R. P., Proc. R. Soc. London Ser. A: 317, 407 (1970).
10. Davis, D. D., Wong, W., and Lephardt, J., Chem. Phys. Lett. 22, 273 (1973).
11. Bensen, S. W., and Axworthy, A. E., J. Chem. Phys. 42, 2614 (1965).
12. Phillips, L. F. and Schiff, H. I., J. Chem. Phys. 36, 1509 (1962).
13. Kezenski, D. C., Simonaites, R., Heichlen, J., Intern. J. Chem. Kinetics 3, 467 (1971).
14. Biendenkapp D. and Bair, E. J., J. Chem. Phys. 52, 6119 (1970).
15. Biendenkapp, D., Hartshorn, L. G., and Bair, E. J., Chem. Phys. Lett. 5, 379 (1970).
16. Snelling, D. R. and Bair, E. J., J. Chem. Phys. 47, 228 (1967).
17. Heidner, R. F. and Husain, D., Chem. Soc. Far. II 69, 927 (1973).
18. Gilpin, R., Schiff, H. I., and Welge, K. H., J. Chem. Phys. 55, 1087 (1971).
19. Giachardi, D. J. and Wayne, R. P., Proc. R. Soc. London, Ser. A: 330, 131 (1972).
20. Young, R. A., Black, G., and Slinger, T. G., J. Chem. Phys. 49, 4758 (1968).
21. Noxon, J. F., J. Chem. Phys. 52, 1852 (1970).
22. Izod, T. P. J. and Wayne, R. P., Proc. Royal Soc. A308, 81 (1968).

23. Filseth, S. V., Zia, A., and Welge, K. H., J. Chem. Phys. 52, 5520 (1970).
24. Becker, K. G., Groth, W., and Schurath, U., Chem. Phys. Lett. 8, 259 (1971).
25. Wayne, R. P. and Pitts, T. N., J. Chem. Phys. 50, 3644 (1969).
26. Becker, K. H., Groth, W., and Schurath, U., Chem. Phys. Lett. 14, 489 (1972).
27. McNeil, R. J. and Cook, G. R., J. Chem. Phys. 47, 5385 (1967).
28. Arnold, S. J. and Ogryzlo, E. A., Can. J. Phys. 45, 2053 (1967).
29. Gauthier, M. and Snelling, D. R., Chem. Phys. Lett. 5, 93 (1970).
30. Findley, F. D., Fortin, C. J., and Snelling, P. R., Chem. Phys. Lett. 3, 203 (1969).
31. Clark, I. D. and Way, R. P., Chem. Phys. Lett. 3, 93 (1969).
32. Steer, R. P., Ackerman, R. A., and Pitts, J. N., J. Chem. Phys. 51, 843 (1969).
33. Camac M. and Vaughan, A., J. Chem. Phys. 34, 460 (1961).
34. Rink, J. P., Knight H. T., and Duff, R. E., J. Chem. Phys. 34, 1942 (1961) and J. Chem. Phys. 36, 572 (1962).
35. Schofield, K. S., Plant. Space. Sci. 15, 643 (1967).
36. Matthews, P. L., Phys. Fluids 2, 170 (1959).
37. Wilson, J., I. Fluid. Mech. 15, 497 (1963).
38. Wray, K. L., J. Chem. Phys. 38, 1518 (1963).
39. Keifer, J. H. and Lutz, R. W., J. Chem. Phys. 42, 1709 (1965).
40. Cherry, S. S., Van Nice, J. J., and Gold, P. I., Pyrodynamics 6, 275 (1968).
41. Kaufman, F. and Kelso, J. R., Discuss, Faraday Soc. 37, 26 (1964).
42. Sauer, M. C. and Dorfman, L. M., J. Amer. Chem. Soc. 87, 3801 (1965).
43. Kaufman, F. and Kelso, J. R., J. Chem. Phys. 46, 4541 (1967).
44. Mulcahy, M. F. R., and Williams, D. J., Trans. Farad. Soc. 64, 59 (1968).
45. Benson, S. W. and Axworthy, A. E., J. Chem. Phys. 26, 1718 (1957).



46. Zaslowsky, J. A., Urbach, H. B., Leighton, F., Wnuk, R. J., and Wojtowicz, J. A., *J. Am. Chem. Soc.* 82, 2682 (1960).
47. Harteck, P., Reeves, R. P., and Manella, G., *J. Chem. Phys.* 29, 1333 (1958).
48. Ford, A. W., and Endow, N., *J. Chem. Phys.* 27, 1156 (1957).
49. Klein, F. S., and Herron, J. T., *J. Chem. Phys.* 41, 1285 (1964).
50. Kistiakowsky, A. B., and Volpi, G. G., *J. Chem. Phys.* 27, 1141 (1957).
51. Kaufman, F., *J. Chem. Phys.* 28, 352 (1958).
52. Westenberg, A. A., and De Haas, N., *J. Chem. Phys.* 40, 3087 (1964).
53. Ogryzlo, E. A., and Schiff, H. I., *Can. J. Chem.* 37, 1690 (1959).
54. Clyne, M. A. A., and Thrush, B. A., *Proc. Roy. Soc. (London)* A275, 559 (1963).
55. Bates, D. R., "The Earth Plant," ed. G. P. Kuiper, (Univ. of Chicago Press) Ch. 12, 1954.
56. Clyne, M. A. A., McKenny, D. J., and Thrush, B. A., *Trans. Farad. Soc.* 61, 270 (1965).
57. Johnston, H. S., *Nat. Stand. Ref. Data Ser., Nat. Bur. Stand., NSRDS-NBS20* (1968).
58. Morgan, J. E., and Schiff, H. I., *Can. J. Chem.* 41, 903 (1963).
59. Day, M. J., Thompson, K., and Dixon-Lewis, G., *14th Symp. (Int.) on Combustion* 47, (1973).
60. Clyne, M. A. A., and Thrush, B. A., *Proc. Roy. Soc. (London)* A275, 544 (1963).
61. Westenberg, A. A., and De Haas, N., *J. Chem. Phys.* 46, 490 (1967).
62. Wong, E. L., and Potter, A. E., *J. Chem. Phys.* 43, 3371 (1965).
63. Schott, G. L., Getzinger, R. W., and Seitz, W. A., *Int. J. Chem. Kin.* 6, 921 (1974).
64. Schofield, K., *J. Phys. Chem. Ref. Data* 2, 25 (1973).
65. Elias, L., and Schiff, H. I., *Can. J. Chem.* 38, 1657 (1960).
66. Bonanno, R. A., Kim P., Lee, J., and Timmons, R. B., *J. Chem. Phys.* 57, 1377 (1972).

67. Herron, J. T., and Penzhorn, R. D., J. Phys. Chem. 73, 191 (1969).
68. Herron, J. T., and Huie, R. E., J. Phys. Chem. 73, 1326 (1969).
69. Herron, J. T., and Huie, R. E., J. Phys. Chem. 73, 3327 (1969).
70. Snuggs, R. M., et al., Phys. Rev. A3, 487 (1971).
71. McKnight, L. G., Phys. Rev. A., 2, 762 (1970).
72. Cosby, P. C., et. al., J. Chem. Phys. 69, 2771 (1978).
73. Lawton, S. A. and Phelps, A. V., J. Chem. Phys. 69, 1055 (1978).
74. Mauer, J. L. and Schultz, G. T., Phys. Rev. A. 7, 593 (1973).
75. Mathias, R. F. , J. Chem. Phys. 61, 4274 (1974).
76. Greaves, J. C., and Linnett, J. W., Trans. Farad. Soc. 54, 1323 (1958).
77. Greaves, J. C., and Linnett, J. W., Trans. Farad. Soc. 55, 1355 (1959).
78. Greaves, J. C., and Linnett, J. W., Trans. Farad. Soc. 55, 1355 (1959).
79. Linnett, J. W., and Marsden, D. G. H., Proc. Roy. Soc. A234, 489 (1956).
80. Linnett, J. W., and Marsden, G. G. H., Proc. Roy. Soc. A234, 504 (1956).
81. Kaufman, E., Progr. Reaction Kinetics, 1, (1961).
82. Golden, J. A. and Myerson, A. L., J. Chem. Phys. 28, 978 (1958).
83. Williams, D. J., and Mulcahy, M. F. R., Aust. J. Chem. 19, 2163 (1966).
84. Kaufman, F., Proc. Roy. Soc. A247, 123 (1958).
85. Mearns, A. M., and Morris, A. J., J. Phys. Chem. 74, 3999 (1970).
86. Verhoek, F. H., and Daniels, F., J. Amer. Chem. Soc. 53, 1250 (1931).
87. Steese, C. M., and Whittaker, A. G., J. Chem. Phys. 24, 776 (1956).
88. Seshadri, D. N., Fiswanath, D. S., and Juloor, N. R., AIChE J. 16, 420 (1970).
89. Giaugue, W. F., and Kemp, J. D., J. Chem. Phys. 6, 40 (1938).

90. Arnold, S. J., Finlayson, N., and Ogryzlo, E. A., J. Chem. Phys. 44, 2529 (1966).
91. Derwent, R. G., and Thrush, B. A., J. C. S. Farlay II 68, 720 (1972).
92. Derwent, R. G., and Thrush, B. A., Chem. Phys. Lett. 9, 591 (1971).
93. Wayne, R. P., Adv. Photochem; 1 311 (1969).
94. Asmussen, J., Mallavarpu, R., Hamann, J. R., and Park, H. C., Proc. I.E.E.E. 62, 109 (1974).
95. Mertz, S. F., Asmussen, J., and Hawley, M. C., I.E.E.E. Trans. Plasma Science PS-2, 297 (1974).

APPENDIX

```

C
C      MAIN PROGRAM FOR THE CSTR MODEL OF THE PLASMA
C
C      DEFINE VARIABLES:
C      K1,K2,K3,K4, KW  = RATE CONSTANTS
C      FO2              = OXYGEN FLOW RATE
C      D                = DISCHARGE TUBE DIAMETER
C      T                = TEMPERATURE
C      GAMMA            = RECOMBINATION COEFFICIENT
C      RLENGTH          = PLASMA LENGTH
C      RNAV              = AVOGADRO'S NUMBER
C      GC               = CONSTANT
C      VP               = PLASMA VOLUME
C      RLAM             = DIFFUSION LENGTH
C      RVELCO           = RANDOM VELOCITY
C      EOP              = E/P
C      PDENSE           = POWER DENSITY
C      P                = PRESSURE
C      EDENSE           = ELECTRON DENSITY
C      CONVER           = CONVERSION
C      RMAXC            = MAXIMUM CONVERSION
C      MAXY             = MAXIMUM YIELD
C      X                = CONVERSION
C
C      PROGRAM PLASMA (INPUT, OUTPUT, TAPE60=INPUT,TAPE61=
1  OUTPUT)
C      REAL K1,K2,K3,K4,KW
C      COMMON K4
C      DIMENSION FOX(16)
C
C      SET THE O2 FLOW RATES TO BE USED
C
C      DATA FOX/1.0E-05,2.5E-05,5.0E-05,7.5E-05,1.0E-04,
1  1.5E-04,2.0E-04,2.5E-04,3.0E-04,3.5E-04,4.0E-04,
1  4.5E-04,5.0E-04,6.0E-04,7.0E-04,8.0E-04/
C
C      SET TUBE DIAMETER,TEMPERATURE,RECOMBINATION COEFFICIENT
C      PLASMA LENGTH,CONSTANT
C
C      D=1.8 $ T=298.0 $ GAMMA=1.6E-04 $ RLENGTH=8.0
C      PI=3.141592654 $ RNAV=6.02252E+23 $ GC=32.174
C
C      CALCULATE PLASMA VOLUME,DIFFUSION LENGTH, RANDOM
C      VELOCITY
C
C      VP=RLENGTH*PI*D**2/4.0
C      RLAM=D/2.0/2.405
C      RVEL=8.0/PI*1.38033E-16*T/16.0*RNAV*GC*7.37562E-08
1  *453.59237*929.0304
C      RVELOC=SQRT(RVEL)

```

```

C
C   SET RATE CONSTANTS AS A FUNCTION OF TEMPERATURE
C
      K2=3.9704E-32/SQRT(T)
      K3=2.5894E-33/SQRT(T)
      K4=1.9E-35*EXP(2100./1.98725/T)
      R=62363.32
      KW=RVELOC*GAMMA/D/2.0

C
C   READ VALUES OF PLAMBDA,E/P,ELECTRON DENSITY,K1
C
      DO 15 L=1,6
        POWER=100.0
        READ(60,910) PLAM,EOP,EDEN,K1

C
C   CALCULATE POWER DENSITY,PRESSURE
C
      DO 10 J=1,14
        PDENSE=POWER/VP
        P=PLAM/RLAM
        EDENSE=EDEN*PDENSE*RLAM

C
C   WRITE DISCHARGE PARAMETERS
C   WRITE(61,830) D,VP,EOP,K1,K2,K3,KW EDENSE, GAMMA
C
      WRITE(61,790)

C
C   SET THE O2 FLOW RATE TO BE USED
C
      DO 5 I=1,16
        IFLAG=1
        FO2=FOX(I)

C
C   CALL A REGULA FALSI SUBROUTINE TO SOLVE CSTR RATE
C   EQUATION FOR CONVERSION
C
      CALL REGULA (K1,KW,K2,K3,EDENSE,VP,FO2,P,R,T,
1         RNAV,X,IFLAG)
      CONVER=X

C
C   CALL A REGULA FALSI SUBROUTINE TO SOLVE FOR MAX
C   CONVERSION
C
      IFLAG=2
      CALL REGULA(K1,KW,K2,K3,EDENSE,VP,FO2,P,R,T,
1         RNAV,X,IFLAG)
      RMAXC=X

```

```

C
C
C      CALCULATE YIELD AND MAXIMUM YIELD
      YIELD=2.0*F0*CONVER/POWER*3600000.0
      MAXY=2.0*F02*RMAXC/POWER*3600000.0
      F02=F02*1.0E+06
C
C
C      WRITE CONVERSION AND YIELD FOR THE DISCHARGE
C      PARAMETERS
      WRITE(61,820) P,T,POWER,PDENSE,F02,CONVER,
1      YIELD,RMAXC,MAXY
5      CONTINUE
C
C
C      INCREMENT POWER FOR NEXT CALCULATION
      POWER=POWER+100.0
10     CONTINUE
15     CONTINUE
790    FORMAT(1H0,2X,*PRESSURE*,5X,*TEMP*,5X,*POWER*,5X,
1      *POWER DENSITY*,5X,*O2 FLOW*,5X,*CONVERSION*,5X,
1      *YIELD*,5X,*MAX CONVERSION*,5X,*MAX YIELD*)
820    FORMAT(1H0,3X,F5.3,7X,F5.1,4X,F6.1,7X,F8.4,9X,F5.1,
1      8X,F6.4,7X,F7.4,8X,F6.4,11X,F7.4)
830    FORMAT(1H1,*DIAMETER=*,F6.4,/,*PLASMA VOLUME=*,
1      F7.4,/,*E/P=*,F6.2,/,*K1=*,E10.4,/,*K2=*,E10.4,/,
1      *K3=*,E10.4,/,*KW=*,E10.4,/,*ELECTRON DENSITY=*,
1      E12.6,/,*GAMMA=*,E10.4)
910    FORMAT(F10.4,F10.2,F14.1,F20.15)
      END
C
C
C      REGULA FALSI SUBROUTINE SEARCHES FOR THE CONVERSION
C
C      SUBROUTINE REGULA(K1,KW,K2,K3,EDENSE,VP,F02,P,R,T,
1      RNAV,X,IFLAG)
      REAL K1,K2,K3,K4,KW
      L=0
C
C
C      SET LEFT AND RIGHT LIMITS OF X AND MAXIMUM ERROR
      XL=1.0 $ XR=0.0 $ ITMAX=100 $ ERR=1.0E -6
C
C
C      BEGIN SEARCH FOR X
      DO 5 I=1,ITMAX
C
C
C      FIND THE FUNCTION VALUE AT THE LEFT LIMIT
1      CALL FUNC(K1,KW,K2,K3,EDENSE,VP,F02,P,R,T,RNAV,XL,
      ANS,IFLAG)
      FXL=ANS

```

```

C
C      FIND THE FUNCTION VALUE AT THE RIGHT LIMIT
C
1      CALL FUNC(K1,KW,K2,K3,EDENSE,VP,F02,P,R,T,RNAV,XR,
      ANS,IFLAG)
      FXR=ANS
C
C      CALCULATE NEW X BETWEEN XL AND XR
C
      X2=(XL*FXR-XR*FXL)/(FXR-FXL)
C
C      FIND THE FUNCTION VALUE AT THE NEW X
C
1      CALL FUNC(K1,KW,K2,K3,EDENSE,VP,F02,P,R,T,RNAV,X2,
      ANS,IFLAG)
      FX2=ANS
C
C      CHECK FOR CONVERGENCE
C
      IF(ABS(FX2).LE.ERR) GO TO 10
C
C      CHECK THE SIGN OF THE FUNCTION AT X2; IF FX2 HAS THE
C      SAME SIGN AS FXL, SET XL=X2; IF FX2 HAS THE SAME SIGN
C      AS FXR, SET XR=X2
C
      CALL SIGN (FXL,J)
      JFXL=J
      CALL SIGN(FXR,J)
      JFXR=J
      CALL SIGN(FX2,J)
      JFX2=J
      IF(JFXL-JFX2).EQ.0) XL=X2
      IF(JFXR-JFX2).EQ.0) XR=X2
      L=L+1
5      CONTINUE
C
C      CONVERGENCE OBTAINED, SET X=X2
C
      X=X2
      IF(L.EQ.100) WRITE(61,800)
800  FORMAT(1H0,* NO CONVERGENCE OBTAINED*)
      RETURN
      END
C
C      SUBROUTINE SIGN CHECKS THE SIGN OF AN INPUT NUMBER
C
      SUBROUTINE SIGN (X,J)
      IF(X.LE.0.0) J=-1
      IF(X.GT.0.0) J= 1
      RETURN
      END

```

```

C
C
C      SUBROUTINE FUNC CONTAINS THE CSTR MATERIAL BALANCE
C
C      SUBROUTINE FUNC(K1,KW,K2,K3,EDENSE,VP,F02,P,R,T,RNAV,
1      X,ANS,IFLAG)
C      REAL K1,K2,K3,K4,KW
C      COMMON K4
C      C1 AND C2 ARE TERMS IN THE CSTR MATERIAL BALANCE
C
C      C1=(1.0-X)/(1.0+X)
C      C2=2.0*X/(1.0+X)
C      C3=R/R/T
C      IF(IFLAG.EQ.2) TO TO 5
C
C      ANS1 IS THE CSTR MATERIAL BALANCE, ANS2 IS THE CSTR
C      MATERIAL BALANCE FOR MAXIMUM CONVERSION.
C
C      ANS1=(2.0*K1*EDENSE*C1*C3-2.0*K2*C2**2*C3**3*RNAV**2
1      *C1-2.0*K3*C2**3*C3**3*RNAV**2-2.0*KW*C2*C3-K4*C2*
1      C1**2*C3**3*RNAV**2)*VP-2.0*F02*X
C      GO TO 10
C      ANS2=2.0*K1*EDENSE*C1*C3-2.0*K2*C2**2*C3**3*RNAV**2
5      *C1-2.0*K3*C2**3*C3**3*RNAV**2-2.0*KW*C2*C3-K4*C2*
1      C1**2*C3**3*RNAV**2
10     CONTINUE
C      IF(IFLAG.EQ.1) ANS=ANS1
C      IF(IFLAG.EQ.2) ANS=ANS2
C      RETURN
C      END
C
C
C      MAIN PROGRAM FOR THE PLUG FLOW MODEL OF THE PLASMA
C
C      DEFINE VARIABLES:
C      K1,K2,K3,K4,KW      = RATE CONSTANTS
C      F02                  = OXYGEN FLOW RATE
C      D                    = DISCHARGE TUBE DIAMETER
C      T                    = TEMPERATURE
C      GAMMA                = RECOMBINATION COEFFICIENT
C      RLENGTH              = PLASMA LENGTH
C      RNAV                 = AVOGADRO'S NUMBER
C      GC                   = CONSTANT
C      VP                   = PLASMA VOLUME
C      RLAM                 = DIFFUSION LENGTH
C      RVELOC               = RANDOM VELOCITY
C      EOP                  = E/P
C      PDENSE               = POWER DENSITY
C      P                    = PRESSURE
C      EDENSE               = ELECTRON DENSITY
C      Y                    = CONVERSION
C      X                    = MOLE FRACTION OF O2
C      FOVP                 = F02/VP

```

```

C
1   PROGRAM PLASMA(INPUT,OUTPUT,TAPE60=INPUT,TAPE61=
      OUTPUT)
      REAL K1,K2,K4,KW,MAXY
      DIMENSION FOX(16)
C
C   SET FOR O2 FLOW RATES TO BE USED
C
      DATA FOX/1.0E-05,2.5E-05,5.0E-05,7.5E-05,1.0E-04,
1     1.5E-04,2.0E-04,2.5E-04,3.0E-04,3.5E-04,4.0E-04,
1     4.5E-04,5.0E-04,6.0E-04,7.0E-04,8.0E-04/
C
C   SET TUBE DIAMETER, TEMPERATURE, RECOMBINATION COEFFICIENT,
C   PLASMA LENGTH, CONSTANTS
C
      D=1.8 $ T=298.0 $ GAMMA=1.6E-04 $ RLENGTH=8.0
      PI=3.141592654 $ RNAV=6.02252E+23 $ GC=32.174
C
C   CALCULATE DIFFUSION LENGTH, RANDON VELOCITY
C
      RLAM=D/2.0/2.405
      RVEL=8.0/PI*1.38033E-16*T/16.0*RNAV*GC*7.37562E-08
1     *453.59237*929.0304
      RVELOC=SQRT(RVEL)
C
C   SET RATE CONSTANTS AS A FUNCTION OF TEMPERATURE
C
      K2=3.9704E-32/SQRT(T)
      K3=2.5894E-33/SQRT(T)
      K4=1.9E-35*EXP(2100./1.98725/T)
      R=62363.32
      KW=RVELOC*GAMMA/D
C
C   READ VALUES OF PLAMBDA,E/P,ELECTRON DENSITY,K1
C
      READ(60,910) PLAM,EOP,EDEN,K1
      PDENSE=2.0
      P=PLAM/RLAM
      C1=R/R/T*RNAV
      DO 10 J=1,10
          EDENSE=EDEN*PDENSE*RLAM
C
C   WRITE DISCHARGE PARAMETERS
C
      WRITE(61,830) D,EOP,K1,K2,K3,K4,KW,EDENSE,GAMMA
      WRITE(61,790)
C
C   SET THE O2 FLOW RATE TO BE USED
C
      DO5 I=1,12
          Y=0.0
          F02=FOX(I)
C

```

```

C      SET THE CONVERSION AND CALCULATE MOLE FRACTION
C
      DO 3 K=1,9
      Y=Y+0.1
      X=2.0*Y/(1.0+Y)
C
C      SET THE NUMBER OF INTERVALS FOR THE NUMERICAL INTEGRATION
C      AND CALL THE INTEGRATION SUBROUTINE TO DETERMINE THE
C      PLASMA VOLUME FOR THE GIVEN CONDITIONS
C
      N=100
      IFLAG=1
      CALL INTEG(K1,KW,K2,K3,EDENSE,VP,F02,P,R,T,RNAV,
1      X,ANS,FLAG,C1,N)
      IF(IFLAG.EQ.1) GO TO 20
      POWER=1.0 $ FOVP=1.0 $ VP=1.0 $ YIELD=1.0
      GO TO 30
C
C      CALCULATE THE INPUT POWER,YIELD,AND O2 FLOW/PLASMA VOLUME.
C      WRITE THE RESULTS.
C
20     POWER=PDENSE*VP
      YIELD=2.0*F02*Y/POWER*3600000.0
      FOVP=F02/VP
30     WRITE(61,820) P,T,POWER,PDENSE,F02,FOVP,VP,Y,
1     YIELD
      3     CONTINUE
      5     CONTINUE"
C
C      INCREMENT POWER DENSITY
C
      PDENSE=PDENSE*2.0
10     CONTINUE
790    FORMAT(1H0,2X,*PRESSURE*,5X,*TEMP*,10X,*POWER*,5X
      *POWER DENSITY*,5X,*O2 FLOW*,5X,*F/V*,10X,
      *PLASMA VOLUME*,5X,*CONVERSION*,5X,*YIELD*)
820    FORMAT(1H0,3X,F5.3,7X,F5.1,3X,E12.6,7X,F7.2,8X,E10.4.
1     2X,E11.5,4X,E12.6,8X,F5.3,8X,F7.4)
830    Format(1H1,*DIAMETER=*,F6.4,/,*E/P=*,F6.2,/,*K1=*,
1     E10.4,/,*K2=*,E10.4,/,*K3=*,E10.4,/,*K4=*,E10.4,
1     /,*KW=*,E10.4,/,*ELECTRON DENSITY=*,E12.6,/,
1     *GAMMA=*,E10.4)
910    FORMAT(F10.4,F10.2,F15.1,F20.15)
      END
C
C      SUBROUTINE INTEG USES SIMPSON'S RULE TO INTEGRATE THE
C      PLUG FLOW MATERIALS BALANCE
C
      SUBROUTINE INTEG(K1,KW,K2,K3,EDENSE,VP,F02,P,R,T,RNAV,
1     B,ANS,IFLAG,C1,N)
      REAL K1,K2,K3,K4,KW

```

```

DIMENSION ANSWER(2)
COMMON K4
A=0.0

C
C
C
BEGIN INTEGRATION

DO 30 J=1,2
SUM=FX(K1,KW,K2,K3,EDENSE,VP,F02,P,R,T,RNAV,B,ANS,
1   IFLAG,C1)-FX(K1,KW,K2,K3,EDENSE,VP,F02,P,R,T,RNAV,
1   A,ANS,IFLAG,C1)
H=(B-A)/N
NE=N/2
NO=2*NE-1
DO 15 I=1,NE
XEVEN=A+2.0*H*(I-1)
SUM=SUM+2.0*FX(K1,KW,K2,K3,EDENSE,VP,F02,P,R,T,
1   RNAV,XEVEN,VAL,IFLAG,C1)
15 CONTINUE
DO 20 I=1,NO,2
XODD=A+H*I
SUM=SUM+4.0*FX(K1,KW,K2,K3,EDENSE,VP,F02,P,R,T,
20  RNAV,XODD,VAL,IFLAG,C1)
CONTINUE
ANSWER(J)=SUM*H/3.0
N=N+100
30 CONTINUE
IF(ABS(ANSWER(1)-ANSWER(2)).LE.0.1) GO TO 40
VP=1.0 $ IFLAG=2
40 ANS=ANSWER(2)
VP=ANS
RETURN
END

C
C
C
THE FUNCTION FX CONTAINS THE FLUG FLOW MATERIAL BALANCE

FUNCTION FX(K1,KW,K2,K3,EDENSE,VP,F02,P,R,T,RNAV,X,VAL,
1   IFLAG,C1)
REAL K1,K2,K3,K4,KW
COMMON K4
C2=1.0-X
DENOM=(2.0*K1*EDENSE*C2-KW*X-2.0*K2*C1**2*X**2*C2
1   -2.0*K3*C1**2*X**3-K4*C1**2*X*C2**2)*(C1*(2.0-X)
1   **2)
FX=(4.0*F02*RNAV)/DENOM
RETURN
END

```

MICHIGAN STATE UNIVERSITY LIBRARIES



3 1293 03178 0525